High-spin states of $^{165,166,167}_{68}$Er populated in incomplete fusion reactions

M. J. Burns,[1,2,*] R. Chapman,[1,2,†] M. Labiche,[1,2,‡] J. Ollier,[1,2,§] V. Kumar,[1,2,‖] C.-J. Lv,[3] Y.-X. Liu,[4] Y. Sun,[3] Th. Kröll,[5,¶] C. Ur,[5,#] K.-M. Spohr,[1,2,#] E. Farnea,[6,**] and T. Martinez[6,††]

[1]*School of Computing, Engineering, and Physical Sciences, University of the West of Scotland, Paisley PA1 2BE, United Kingdom*
[2]*The Scottish Universities Physics Alliance (SUPA), University of Glasgow, Glasgow G12 8QQ, United Kingdom*
[3]*School of Physics and Astronomy, Shanghai Jiao Tong University, Shanghai 200240, China*
[4]*School of Science, Huzhou University, Huzhou 313000, China*
[5]*INFN, Sezione di Padova, and Dipartimento di Fisica, Università di Padova, I35131 Padova, Italy*
[6]*INFN, Laboratori Nazionali di Legnaro, I-35020 Legnaro, Padova, Italy*

(Received 15 April 2025; accepted 11 July 2025; published 11 August 2025)

High-spin states in the $^{165,166,167}_{68}$Er nuclei were populated in the incomplete fusion of 55-MeV ^{7}Li ions with a ^{164}Dy target. Previously known rotational sequences in ^{165,166,167}Er have been extended, in some cases beyond the $i_{13/2}$ two-quasineutron crossing region. In ^{165}Er, four rotational sequences were observed up to a maximum I^{π} of $(45/2^{+})$; in ^{166}Er, five decay sequences were observed to $I^{\pi} = (28^{+})$; and in ^{167}Er, four decay sequences were populated to $I^{\pi} = (53/2^{-})$. Comparisons of the experimental data with the results of Cranked Shell Model calculations provide insight into the configuration dependence of the first two-quasineutron crossing frequencies and the blocking effects of the odd quasineutron in ^{165}Er and ^{167}Er. The experimental high-spin decay sequences in ^{165}Er and ^{167}Er have also been compared with the results of Projected Shell Model (PSM) calculations; the overall agreement between experiment and theory is very good over the complete range of spins for all high-spin rotational sequences. In particular, the observed signature splitting in the $5/2^{+}[642]$ band in ^{165}Er and in the $7/2^{+}[633]$ and $1/2^{-}[521]$ bands in ^{167}Er together with the absence of signature splitting in the high-K $11/2^{-}[505]$ band in ^{165}Er are reproduced in the PSM calculations. For ^{166}Er, the Triaxial Projected Shell Model calculations yield satisfactory results for both the ground and γ-vibrational band. For the latter band, there is a one-to-one correspondence between the theoretical results and experimental data for all states with I^{π} in the range from the 2^{+} bandhead to the 21^{+} state.

DOI: 10.1103/247g-wqd5

I. INTRODUCTION

The study of high-spin states of neutron-rich rare-earth nuclei is experimentally demanding; the vast region of unexplored neutron-rich rare-earth nuclei cannot be accessed using conventional heavy-ion-induced fusion-evaporation reactions with stable beams. Such reactions can, more readily, be used to populate nuclei on the proton-rich side of the valley of stability. In relation to the use of fusion-evaporation reactions, of the three isotopes of erbium studied here, ^{165}Er can be studied using the light-ion-induced reactions, $(\alpha, xn\gamma)$ and ^{160}Gd(^{9}Be, $4n\gamma$), whereas ^{166}Er can be accessed using the $(\alpha, 2n\gamma)$ fusion-evaporation reaction. On the other hand, ^{167}Er is too neutron rich to be accessed by such reactions using stable accelerated beams. However, high-spin states of the yrast sequences in the stable ^{166}Er and ^{167}Er isotopes can be populated in Coulomb excitation studies with high-Z projectiles. Yet another approach to studies of high-spin states of moderately neutron-rich nuclei involves the use of deep-inelastic reactions. In contrast, the approach adopted here involves the use of incomplete fusion reactions initiated by a high-intensity beam of stable energetic ^{7}Li ions. This type of reaction process, in which the light ejectile is, for example, a proton, may be considered as equivalent to a fusion-evaporation reaction initiated with a radioactive beam of ^{6}He ions; the additional

*Present address: AWE Aldermaston, Reading RG7 4PR, United Kingdom.
†Contact author: Robert.Chapman@uws.ac.uk
‡Present address: STFC Daresbury Laboratory, Daresbury, Warrington WA4 4AD, United Kingdom.
§Present address: Rapiscan Systems, Prospect Way, Victoria Business Park, Biddulph, Stoke-on-Trent ST8 7PL, United Kingdom.
‖Present address: Department of Physics, University of Lucknow, Lucknow 226007, India.
¶Present address: Institut für Kernphysik, Technische Universität Darmstadt, 64289 Darmstadt, Germany.
#Present address: Extreme Light Infrastructure (ELI-NP) and IFIN-HH, Horia Hulubei National Institute of Physics and Nuclear Engineering, Bucharest-Măgurele RO-077125, Romania.
**Deceased.
††Present address: CIEMAT (Centro de Investigaciones Energeticas, MedioAmbientales y Tecnologicas), Avenida Complutense, 40, E-28040 Madrid, Spain.

Published by the American Physical Society under the terms of the Creative Commons Attribution 4.0 International license. Further distribution of this work must maintain attribution to the author(s) and the published article's title, journal citation, and DOI.

benefit experimentally is that observation of the "spectator" proton results in an improvement in the resolving power of the associated escape-suppressed Ge γ-ray multidetector array. Experimentally, with the combined use of large arrays of escape-suppressed germanium detectors and silicon charged-particle detector telescope arrays with large solid-angle coverage, the incomplete fusion process is a very useful selective method for the study of the high-spin spectroscopy of moderately neutron-rich nuclei and corresponds to a very early step toward advancing the exploration of the vast region of unexplored neutron-rich nuclei.

Moderately neutron-rich rare-earth nuclei around $A =$ 160–170 have been the subject of numerous experimental and theoretical investigations. Indeed, at the present time, there is much interest in the spectroscopy of neutron-rich nuclear systems. In lighter nuclei, changes to shell structure have been observed, believed to be associated with the monopole part of the tensor interaction between neutron-proton spin-orbit partners, and new magic numbers have been discovered [1]. As the neutron drip line is approached, coupling to the continuum is predicted to result in a softening of the nuclear potential, accompanied by a consequent weakening of the spin-orbit interaction and resulting in changes to shell structure [2]. The description of nuclei near the drip lines is one of the main challenges of current nuclear theory, which was mainly developed to describe the structure of well-bound nuclei. For the isotopes of Er, the neutron drip line lies about 40 neutrons from the most neutron-rich isotope studied experimentally to date. One does not, therefore, expect to see effects resulting from coupling to the continuum in currently accessible Er isotopes. Nevertheless, the experimental study of even moderately neutron-rich nuclei presents an experimental challenge and is a necessary very early step to advancing the exploration of the vast region of unexplored neutron-rich nuclei and can guide theory in the extrapolation to the unexplored nuclear territory.

In sharp contrast to the well-known yrast-band systematics of the lighter even-A isotopes of erbium (see, for example, Ref. [3]), where sharp backbends are present, corresponding to Coriolis-induced two-quasiparticle alignment, the $N =$ 98 ^{166}Er nucleus, studied in the present work, exhibits completely different behavior. The interaction strength between the ground-state band and the crossing two-quasineutron band is known to oscillate as a function of neutron number; the first such observation, for the isotopes of Yb, was made by Hartley *et al.* [4], and discussed there within the context of a deformed shell gap at $N = 98$. The observed effect [4] was subsequently discussed by Faessler *et al.* [5] within the context of angular momentum and particle number projected deformed BCS trial wave functions. ^{166}Er, with neutron number $N = 98$, lies at a peak in interaction strength, resulting in a smooth transition in the crossing of the ground-state band and the two-quasineutron band which, in this case, is based on a pair of neutrons originating from the spherical $i_{13/2}$ shell-model state.

The current study involves the investigation of the high-spin structure of ^{165,166,167}Er produced in incomplete fusion reactions. The experimental data have been compared with the results of Cranked Shell Model calculations. The experimental high-spin decay sequences in ^{165}Er, ^{166}Er, and ^{167}Er have also been compared with the results of Projected Shell Model (PSM) calculations; satisfactory agreement between experiment and theory is obtained over the complete range of spins for all high-spin rotational sequences observed here.

II. EXPERIMENTAL DETAILS AND DATA ANALYSIS

The ^{164}Dy(^{7}Li, $p(d,t,\alpha)xn\gamma$) reactions were studied at the INFN, Legnaro National Laboratory, Italy. The XTU Tandem Van de Graaff accelerator was used to accelerate ^{7}Li ions to an energy of 55 MeV. The isotopically enriched ^{164}Dy (95.6%) target was of thickness 3.5 mg cm^{-2}. Gamma rays emitted from the final nuclei populated in the reaction were detected using the GASP array of 40 escape-suppressed hyperpure n-type Germanium (HPGe) detectors and an 80-element inner bismuth germanate (BGO) ball, which acts as a multiplicity filter and total energy spectrometer [6,7]. The average Ge energy resolution at 1332 keV (^{60}Co) was better than 2.3 keV FWHM and the relative efficiency of each crystal was about 80%. The ISIS silicon charged-particle detector array [8] was located inside the spherical target chamber of the GASP Ge array. The silicon array consists of 40 E-ΔE detectors; the ΔE detectors are of thickness 130 μm while the E detectors are 1 mm thick. The energy loss and total energy information is used to identify the nature of the light emitted particles (p, d, t, α particles) and therefore acts as a filter to select the isotopes of interest during data analysis. The high efficiency and resolving power of the GASP multidetector γ-ray array coupled with the selectivity provided by the ISIS array yielded good statistics and excellent channel selection. Experimental data were taken during a 5-day run. The trigger conditions for an "event" corresponded to two or more Ge signals and two or more BGO inner-ball element signals. The γ-ray data were subsequently gain matched and sorted into an E_γ-E_γ-E_γ cube using the sort code gavsort [9], and the coincident data obtained with ISIS were sorted into a ΔE-E matrix. The ^{165,166,167}Er reaction channels were selected by setting a software condition on the "spectator" charged particles detected in ISIS (see Fig. 1). The γ-γ-γ cubes were analyzed using programs from the RADWARE [10] analysis package. Gamma-ray coincidence spectra were created initially by gating on previously known transitions belonging to ^{165,166,167}Er. Energy and efficiency calibrations of the Ge detectors were made with radioactive sources of ^{133}Ba and ^{152}Eu. Level schemes of the populated nuclei resulted from an analysis of γ-γ-γ cubes using the LEVIT8R [10] computer code. In the absence of γ-ray angular correlation measurements, all spin and parity assignments of hitherto unobserved states are based on the usual assumption that they follow the expected behavior with increasing excitation energy within well-developed rotational sequences; consequently, new spin and parity assignments should be considered tentative and they appear in parentheses in the level schemes and tables presented here. One of the advantages of the incomplete fusion reaction is that it is highly selective; only a few isotopes are significantly populated, namely, ^{165,166,167}Er and ^{165}Ho in the present case, of which ^{166}Er, produced in the $p4n$, $d3n$, and $t2n$ exit channels, is the strongest.

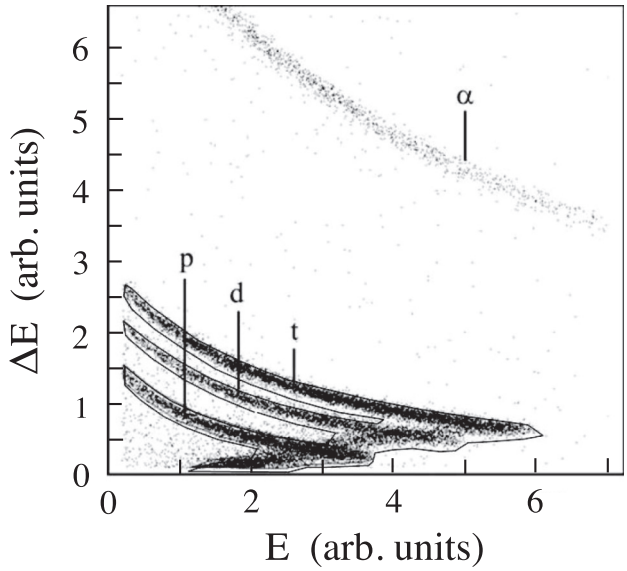


FIG. 1. Energy loss ΔE (arbitrary units) as a function of residual energy E (arbitrary units) for charged particles detected in the ISIS ΔE-E Si detector array.

III. EXPERIMENTAL RESULTS

A. Previous work

States of ^{165}Er have previously been studied using nucleon stripping and pickup reactions and in (α, $xn\gamma$) fusion-evaporation reactions [11–13]. In the (α, $xn\gamma$) work, the ground-state band, based on the $5/2^-[523]$ single-neutron Nilsson orbital, was observed to spin $11/2^-$ and was very weakly populated. States of the rotational sequences based on the $3/2^-[521]$ Nilsson configuration were observed to decay to the ground-state band. The rotational sequence based on the $5/2^+[642]$ state was very strongly populated and observed to spin $25/2^+$ (tentatively to $29/2^+$). The half-life of the $11/2^-[505]$ state, at 551 keV [12], was measured to be 0.25(3) μs [13] and the rotational sequence based on this state was populated to spin $17/2^-$. In the more recent work of Wang *et al.* [14], the rotational sequences based on the $5/2^-[523]$, $11/2^-[505]$, and $5/2^+[642]$ Nilsson bandheads were populated to spins $(45/2^-)$, $(31/2^-)$, and $(49/2^+)$, respectively, using the ^{160}Gd(^{9}Be, $4n$) fusion-evaporation reaction. In addition, Wang *et al.* [15] identified a "band" consisting of two levels, both of which decay strongly to the $11/2^-[505]$ band, and assigned it as the γ-vibrational band built on the $11/2^-[505]$ configuration. A previously unobserved level at an excitation energy of 1823 keV has also been proposed to be a three-quasiparticle state [15]. Isomeric states in the ^{164}Er region were also studied by Swan *et al.* [16] using ^{9}Be + ^{160}Gd reactions. In addition to the previously known 551-keV isomeric state in ^{165}Er, a new isomer ($I = (19/2)$) at 1823.0(2) keV was identified with a half-life of 0.37(4) μs; the 1823.0(2)-keV level had previously been observed by Wang *et al.* [15], as noted above.

Prior to the present work, the ^{166}Er nucleus was studied using the (α, $2n\gamma$) reaction [17–19] and by Coulomb excitation (for example, Ref. [20]). The yrast sequence was established to spin (16^+) [19,20] and the γ-vibrational band to spins (13^+) and (14^+) [19]. The ^{166}Er nucleus was also populated in the deep-inelastic experiments of Ollier [21]; 230-MeV ^{36}S ions were incident on a thick ^{176}Yb target and the γ decay of the populated final nuclei was studied using the GASP multidetector array. The yrast decay sequence was extended to a tentative spin of (26^+).

The energy levels of ^{167}Er have been studied in the β decay of ^{167}Ho [22] and by Coulomb excitation using beams of ^{16}O ions [23], ^{35}Cl ions [24], and ^{209}Bi ions [25]. The ground-state rotational sequence, based on the $i_{13/2}$ neutron intruder orbital, was identified to spin $(37/2^+)$ [25] and lifetimes of the $(9/2^+)$ to $(25/2^+)$ levels were measured using the Doppler shift attenuation method [24]. Decay sequences based on the $1/2^-[521]$ and $5/2^-[512]$ single quasineutron excitations were established to spins $(37/2^-)$ and $(27/2^-)$, respectively. The rotational sequence based on the $5/2^-[523]$ Nilsson configuration was populated to low spin $(7/2^-)$ [22]. The $K \pm 2$ γ-vibrational structures were populated to spins $7/2^+$ and $(11/2^+)$ [23]. The $K^\pi = (11/2^+)$ γ-vibrational band, based on the parallel coupling of a $K = 2$ phonon with the ground-state $K = 7/2$ unpaired neutron, was extended from spin $(17/2^+)$ to spin $(37/2^+)$ [25].

B. ^{165}Er

The level scheme of ^{165}Er, established in the present work, is presented in Fig. 2. The rotational sequence based on the $5/2^-[523]$ Nilsson state, identified in the work of Wang *et al.* [14], was very weakly populated in the present study.

1. The $5/2^+[642]$ rotational sequence

The $5/2^+[642]$ rotational sequence, based on the $1i_{13/2}$ spherical shell-model state, originates from a downward-sloping neutron orbital (energy versus quadrupole deformation diagram). The $\alpha = +\frac{1}{2}$ signature of the rotational sequence, previously known to spin $(49/2^+)$ [14], was observed to spin $(45/2^+)$ in the present work; here, there is good agreement with the level scheme of Wang *et al.* [14]. The γ-ray spectrum of Fig. 3(a) shows the result of the sum of all double gates involving the γ-ray transitions at 141, 225, 306, 384, and 457 keV. The inset in Fig. 3(a) shows a γ-ray spectrum resulting from the sum of all double gates involving the 457-, 523-, and 582-keV transitions. Figure 3(b) shows the γ-ray transitions within the $\alpha = -\frac{1}{2}$ signature of the rotational sequence; the spectrum results from a double gate on the 402- and 569-keV transitions. The inset shows the γ-ray spectrum corresponding to a double gate set on the 402- and 637-keV transitions. The ^{165}Er level scheme of Fig. 2 was based on an analysis of such double-gated γ-ray spectra. The present work confirms the level scheme of the $5/2^+[642]$ rotational sequence to spin $(45/2^+)$ for signature $\alpha = \frac{1}{2}$ and to spin $(39/2^+)$ for signature $\alpha = -\frac{1}{2}$ [14]. The I^π assignments are consistent with the recent Nuclear Data Sheets evaluation [26], which includes members of the rotational sequence for $I^\pi \leqslant (49/2^+)$.

It can be seen that, up to spin $(21/2^+)$, $\Delta I = 1$ transitions depopulate both the favored and unfavored signatures of the

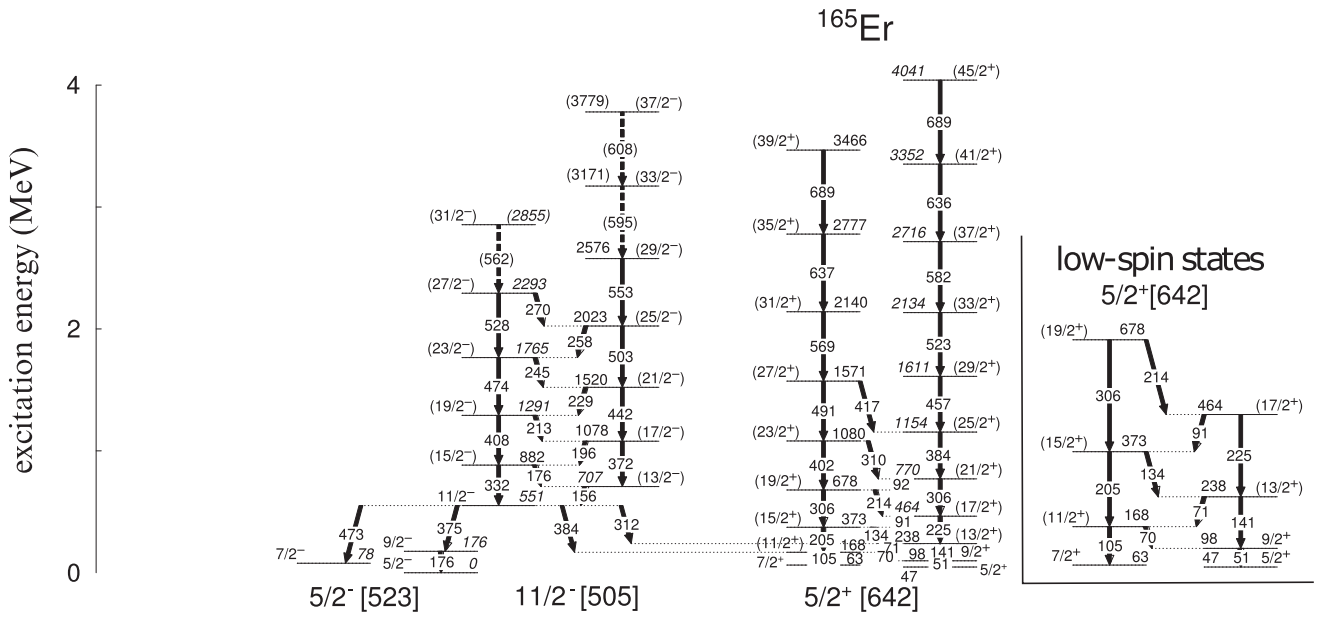


FIG. 2. Level scheme of ^{165}Er from the present work. The I^{π} values are those of Wang *et al.* [15]. The inset shows the lower-spin part of the $5/2^{+}[642]$ decay sequence in more detail. See text for details.

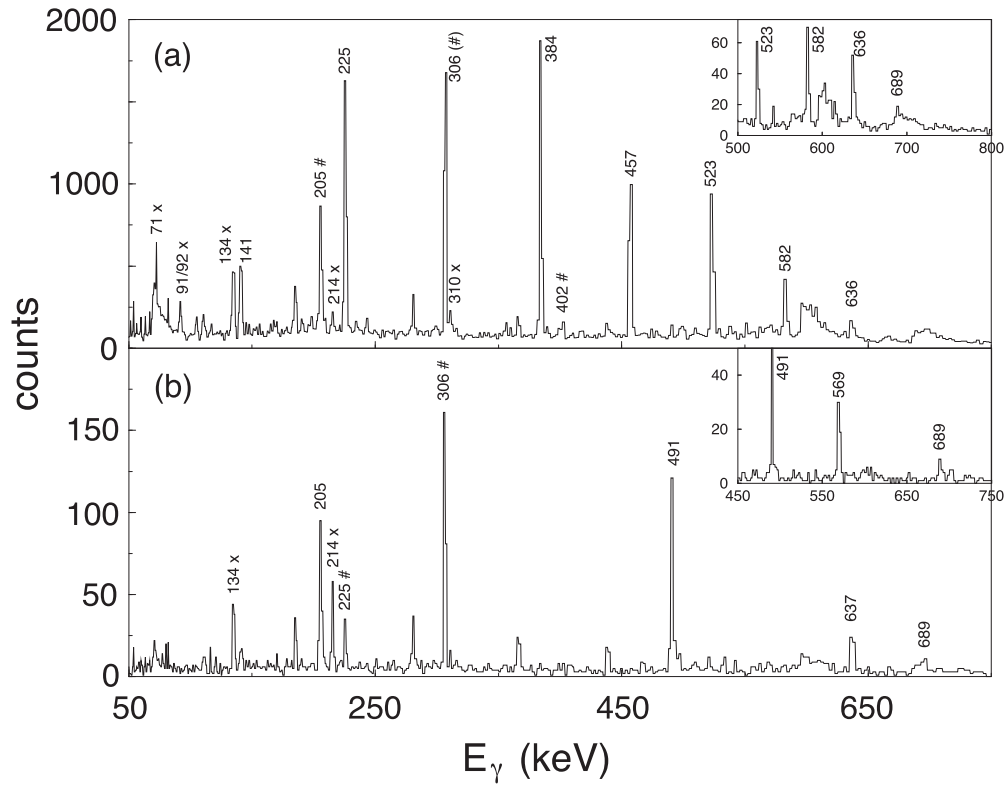


FIG. 3. Gated γ-ray spectra showing transitions within the (a) $\alpha = +\frac{1}{2}$ and (b) $\alpha = -\frac{1}{2}$ signatures of the $5/2^{+}[642]$ rotational sequences of ^{165}Er. For the $\alpha = \frac{1}{2}$ signature of the band, the γ-ray spectrum results from the sum of all double gates involving the γ-ray transitions of energy 141, 225, 306, 384, and 457 keV. The γ-ray spectrum presented in the inset in Fig. 3(a) corresponds to a sum of all double gates involving the 457-, 523-, and 582-keV transitions. For the $\alpha = -\frac{1}{2}$ signature of the band, the γ-ray spectrum results from a double gate involving the γ-ray transitions of 402 and 569 keV, while the γ-ray spectrum presented in the inset in Fig. 3(b) corresponds to a double gate set on the 402- and 637-keV transitions. Peaks marked "x" and "#" correspond to the $\Delta I = 1$ crossing transitions and transitions in the signature partner, respectively. See text for details.

band, whereas, for higher spins, crossing transitions deexcite only toward the favored signature ($\alpha = +\frac{1}{2}$). This is a consequence of the large signature splitting: the $\alpha = +\frac{1}{2}$ to $\alpha = -\frac{1}{2}$ dipole transitions become less likely with increasing spin as a consequence of the decrease in transition energy; eventually, $\Delta I = 1$ transitions are not energetically possible. In the (α, $3n\gamma$) work of Hjorth *et al.* [12], the multipolarities of the $\Delta I = 1$ transitions from states with $I^\pi \leqslant (19/2^+)$ were established as magnetic dipole.

Table I shows the measured relative intensities of the γ-ray transitions in the $5/2^+[642]$ decay sequence and proposed spin and parity assignments.

2. The $11/2^-[505]$ rotational sequence

The $11/2^-[505]$ rotational sequence originates from an upward-sloping neutron orbital in the $1h_{11/2}$ spherical shell-model orbit. As noted above, the $11/2^-$ isomeric state has a half-life of 0.25(3) μs [13]. In the present work, no tight timing conditions were placed during the offline data analysis and the γ-γ timing coincidence window (100 ns) was comparable to the half-life of the state; consequently, the decays of this state to the ground-state band and to the $5/2^+[642]$ rotational sequence are observed here. In relation to the $11/2^-[505]$ rotational sequence established in the work of Wang *et al.* [14], here two additional tentative transitions, $(33/2^-) \rightarrow (29/2^-)$ and $(37/2^-) \rightarrow (33/2^-)$, have been added to the $\alpha = +\frac{1}{2}$ signature of the band. In addition, the energy of the tentative $(31/2^-) \rightarrow (27/2^-)$ transition (562 keV) is in disagreement with the 574-keV transition energy measured by Wang *et al.* [14]. In Fig. 2, apart from the tentative $(33/2^-)$ and $(37/2^-)$ assignments, the I^π assignments are consistent with the recent Nuclear Data Sheets evaluation [26], which includes members of the rotational sequence for $I^\pi \leqslant (31/2^-)$.

The γ-ray spectrum of Fig. 4 is the result of a sum of all double gates involving the previously known $\Delta I = 1\gamma$-ray transitions of energy 156, 176, 196, 213, 229, 245, 258, and 270 keV. The previously observed [14] $\Delta I = 2$ transitions, presumably of $E2$ multipolarity, at energies of 332, 372, 408, 442, 474, 503, 528, and 553 keV, are also observed in the coincidence spectrum, as expected. The inset to Fig. 4 shows a section of the γ-ray spectrum resulting from a double gate on the 408- and 474-keV transitions; the 528-keV photopeak, corresponding to the $(27/2^-) \rightarrow (23/2^-)$ transition, is observed, in addition to a 562-keV transition which here is tentatively assigned to the $(31/2^-) \rightarrow (27/2^-)$ transition. As noted above, in Ref. [14], the energy of the $(31/2^-) \rightarrow (27/2^-)$ transition is given as 574 keV. The upper spectrum of Fig. 5 shows a section of the γ-ray spectrum resulting from a double gate on the 503- and 553-keV transitions. The photopeak at 442 keV corresponds to the $(21/2^-) \rightarrow (17/2^-)$ transition, while those, previously unobserved, at energies of 595 and 608 keV are tentatively assigned to the $(33/2^-) \rightarrow (29/2^-)$ and $(37/2^-) \rightarrow (33/2^-)$ transitions, respectively. In support of these new tentative assignments, the lower spectrum of Fig. 5 shows a section of the γ-ray spectrum resulting from a double gate on the 442- and 553-keV transitions; in this case, the 503-keV transition is observed, in addition to those at energies of 595 and 608 keV.

TABLE I. Relative γ-ray intensities for transitions in the $5/2^+[642]$ and $11/2^-[505]$ rotational sequences in ^{165}Er. See text for details.

E_γ (keV) $5/2^+[642]$	I_i^π	I_f^π	Relative intensity
51	$9/2^+$	$5/2^+$	
141	$(13/2^+)$	$9/2^+$	
225	$(17/2^+)$	$(13/2^+)$	
306	$(21/2^+)$	$(17/2^+)$	1000(53)
384	$(25/2^+)$	$(21/2^+)$	662(15)
457	$(29/2^+)$	$(25/2^+)$	395(13)
523	$(33/2^+)$	$(29/2^+)$	225(7)
582	$(37/2^+)$	$(33/2^+)$	73(4)
636	$(41/2^+)$	$(37/2^+)$	23(1)
689	$(45/2^+)$	$(41/2^+)$	7(1)
105	$(11/2^+)$	$7/2^+$	
205	$(15/2^+)$	$(11/2^+)$	
306	$(19/2^+)$	$(15/2^+)$	
402	$(23/2^+)$	$(19/2^+)$	607(21)
491	$(27/2^+)$	$(23/2^+)$	336(10)
569	$(31/2^+)$	$(27/2^+)$	206(9)
637	$(35/2^+)$	$(31/2^+)$	67(5)
689	$(39/2^+)$	$(35/2^+)$	22(4)
70	$(11/2^+)$	$9/2^+$	
134	$(15/2^+)$	$(13/2^+)$	
214	$(19/2^+)$	$(17/2^+)$	148(6)
310	$(23/2^+)$	$(21/2^+)$	50(4)
417	$(27/2^+)$	$(25/2^+)$	18(3)
$11/2^-[505]$			
156	$(13/2^-)$	$11/2^-$	
176	$(15/2^-)$	$(13/2^-)$	1000(92)
196	$(17/2^-)$	$(15/2^-)$	947(71)
213	$(19/2^-)$	$(17/2^-)$	248(15)
229	$(21/2^-)$	$(19/2^-)$	123(14)
245	$(23/2^-)$	$(21/2^-)$	74(7)
258	$(25/2^-)$	$(23/2^-)$	42(5)
270	$(27/2^-)$	$(25/2^-)$	35(5)
332	$(15/2^-)$	$11/2^-$	
408	$(19/2^-)$	$(15/2^-)$	617(49)
474	$(23/2^-)$	$(19/2^-)$	434(34)
528	$(27/2^-)$	$(23/2^-)$	175(18)
562	$(31/2^-)$	$(27/2^-)$	134(34)
372	$(17/2^-)$	$(13/2^-)$	507(76)
442	$(21/2^-)$	$(17/2^-)$	259(23)
503	$(25/2^-)$	$(21/2^-)$	148(16)
553	$(29/2^-)$	$(25/2^-)$	112(16)
595	$(33/2^-)$	$(29/2^-)$	34(9)
608	$(37/2^-)$	$(33/2^-)$	21(7)

Table I shows relative γ-ray intensities and spin assignments for members of the $11/2^-[505]$ rotational sequence.

C. ^{166}Er

The level structure of ^{166}Er from the present work, based on an analysis of the incomplete fusion reactions ^{164}Dy (^{7}Li, $p4n$), ^{164}Dy (^{7}Li, $d3n$), and ^{164}Dy (^{7}Li, $t2n$), is presented in Fig. 6.

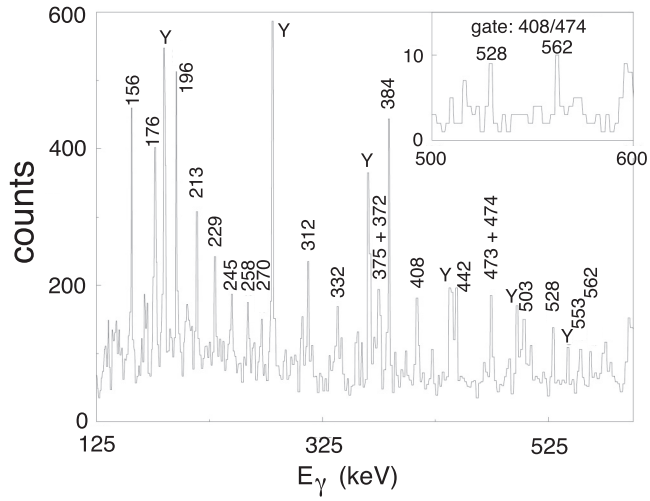


FIG. 4. Gamma-ray spectrum resulting from the sum of all double gates involving the γ-ray transitions of energy 156, 176, 196, 213, 229, 245, 258, and 270 keV within the $11/2^-[505]$ decay sequence of ^{165}Er. The peaks marked "Y" correspond to the yrast decay sequence of ^{166}Er, brought in by the multiple gating. The inset shows a section of the γ-ray spectrum resulting from a double gate on the 408- and 474-keV transitions.

1. *Yrast band*

As noted above, previous publications established the yrast decay sequence to spin 16^+ [19,20]. Figure 7(a) shows a γ-ray spectrum corresponding to a sum of all double gates involving the 184-, 280-, 366-, 438-, 497-, 542-, 578-, 611-, 648-, and 694-keV transitions within the yrast decay sequence of ^{166}Er. The rotational sequence can clearly be seen up to the 694-keV transition, corresponding to the deexcitation of the state with $I^\pi = (22^+)$. In agreement with the unpublished results of Ollier [21], the transitions corresponding to the deexcitation of the (22^+), (20^+), and (18^+) states can be seen at γ-ray energies of 694, 648, and 611 keV, respectively. The inset

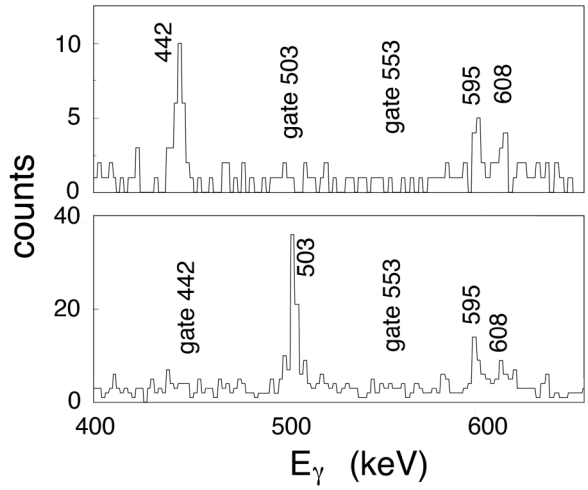


FIG. 5. Gamma-ray spectrum resulting from the sum of double gates set on the 503- and 553-keV transitions of ^{165}Er (top) and on the 442- and 553-keV transitions of ^{165}Er (bottom).

TABLE II. Relative γ-ray intensities for transitions in the Yrast band of ^{166}Er. See text for details.

E_γ (keV)	I_i^π	I_f^π	Relative intensity
81	2^+	0^+	–
184	4^+	2^+	1000(6)
280	6^+	4^+	922(6)
366	8^+	6^+	739(5)
438	10^+	8^+	621(5)
497	12^+	10^+	318(4)
542	14^+	12^+	213(4)
578	(16^+)	14^+	108(17)
611	(18^+)	(16^+)	57(16)
648	(20^+)	(18^+)	24(9)
694	(22^+)	(20^+)	14(9)
750	(24^+)	(22^+)	5.5(6)
810	(26^+)	(24^+)	2.4(5)
(874)	(28^+)	(26^+)	2.1(5)

to Fig. 7(a) shows a partial γ-ray spectrum corresponding to a double gate on the 648- and 694-keV transitions. The spectrum shows clear evidence for the deexcitation of the proposed (24^+) state to the (22^+) state via a 750-keV γ-ray transition. In addition, there is evidence for the deexcitation of the proposed (26^+) state via an 810-keV transition; this is in agreement with the tentative assignment by Ollier [21] of a transition of energy 812 keV. In the present work, the 874-keV γ-ray transition is a further tentative extension to the yrast band, corresponding to the deexcitation of a proposed (28^+) level at 7354 keV.

The in-band γ-ray transitions were ordered according to relative intensity measurements as presented in Table II. Transition intensities for the states up to spin 14^+ in the yrast band were measured directly from the total-projection γ-ray spectrum. For higher-lying transitions in the yrast band, intensities were measured using an appropriate combination of double gates. Intensities were then normalized to those taken from the total-projection spectrum.

2. *γ-vibrational band*

The spectrum of Fig. 7(b) shows γ-ray transitions (marked #) within the $\alpha = 0$ signature of the rotational sequence based on a single γ-vibrational phonon. The spectrum is the result of a sum of all double gates on γ rays of energy 338, 409, 468, 517, 562, and 608 keV, and shows γ-ray decay within the rotational sequence to spin (22^+). Four new transitions have been added to the previous work of Fields *et al.* [19] at γ-ray energies of 562, 608, 644, and 674 keV, corresponding to the deexcitation of the proposed (16^+), (18^+), (20^+), and (22^+) excited states. A tentative transition of energy 693 keV has also been included in the decay sequence, corresponding to the deexcitation of the proposed (24^+) state at 6128 keV. The spectra of Figs. 7(b) and 7(c) show strong photopeaks (marked *) corresponding to the deexcitation of the 4^+, 6^+, 8^+, 10^+, 12^+, and 14^+ states of the ground-state band. The inset to Fig. 7(b) presents a γ-ray spectrum corresponding to the sum of all double gates on γ-ray transitions of energy 517, 562, 608, 644, and 674 keV, and shows the proposed

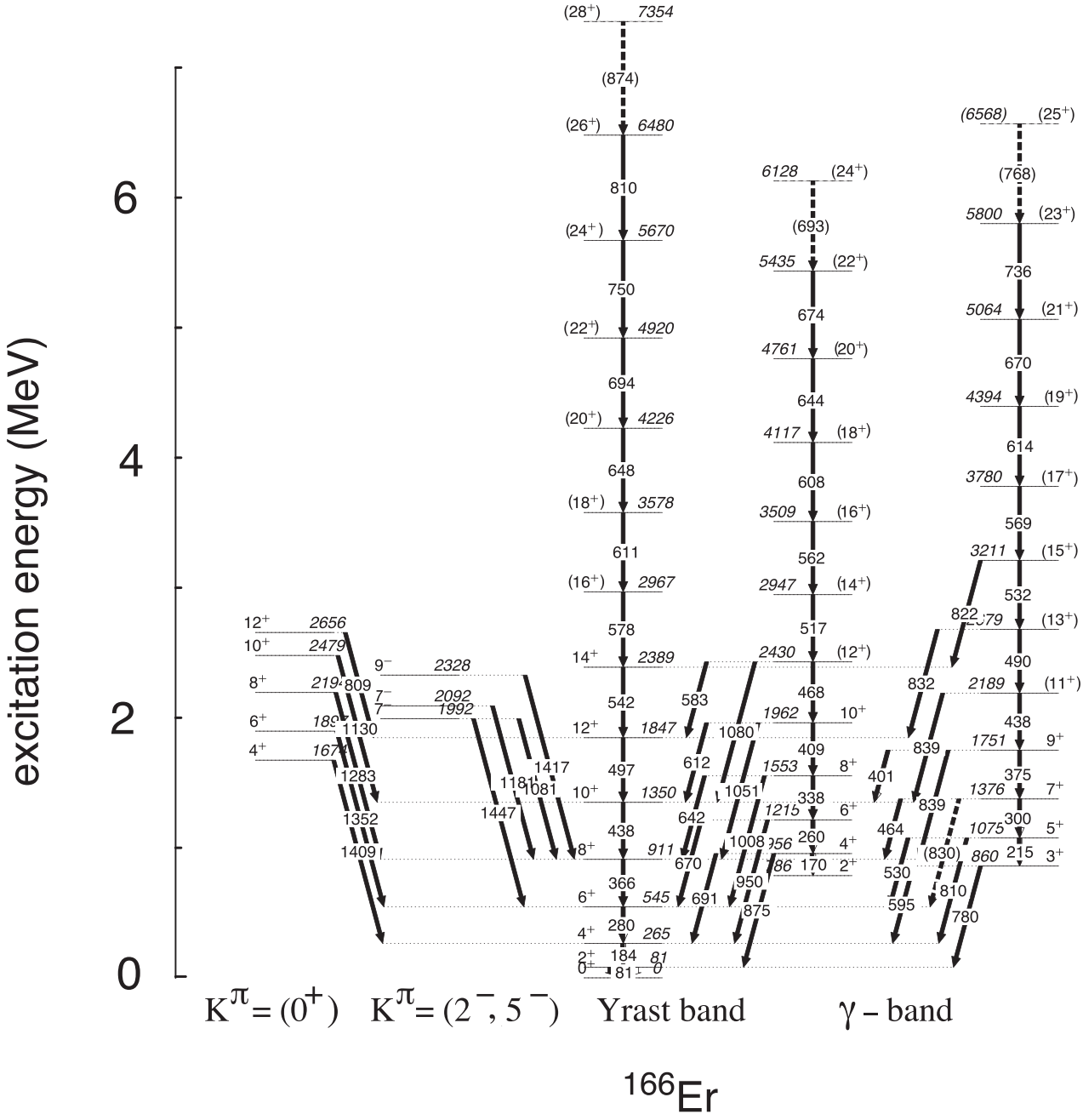


FIG. 6. Level scheme of ^{166}Er from the present work.

$\Delta I = 2$ transitions which connect the previously unobserved high-spin members of the band. Figure 7(c) shows a γ-ray spectrum corresponding to transitions in the $\alpha = 1$ signature of the band, marked #. The spectrum corresponds to a sum of all double gates involving γ-ray transitions of energy 300, 375, 438, 490, 532, 569, and 614 keV. The γ-ray spectrum shows the members of the band up to a tentative spin assignment of (25^+). The rotational sequence can clearly be seen to be extended by five new transitions from spin (13^+) to spin (23^+). The new transitions are at energies of 532, 569, 614, 670, and 736 keV. A tentative addition to the band can also be seen at a γ-ray energy of 768 keV, corresponding to the deexcitation of the proposed (25^+) state at 6568 keV. The spectrum in the inset is the result of a sum of all double gates involving the 490-, 532-, 569-, and 614-keV γ-ray transitions; all new transitions can clearly be seen. The transitions marked "x" in Fig. 7(c) correspond to interband transitions to the yrast sequence. In the paper of Fields *et al.* [19], the deexcitation of the (14^+) state was reported to be via a 451.3-keV γ-ray transition and the decay of the (13^+) state via a 465-keV transition. However, here the spectra of Figs. 7(b) and 7(c) show that the energy of the γ-ray transition associated with the deexcitation of the (14^+) state is 517 keV while the (13^+)-to-(11^+) transition energy is 490 keV.

Table III presents the relative γ-ray intensities and spin assignments for members of the γ-vibrational band ($\alpha = 0$

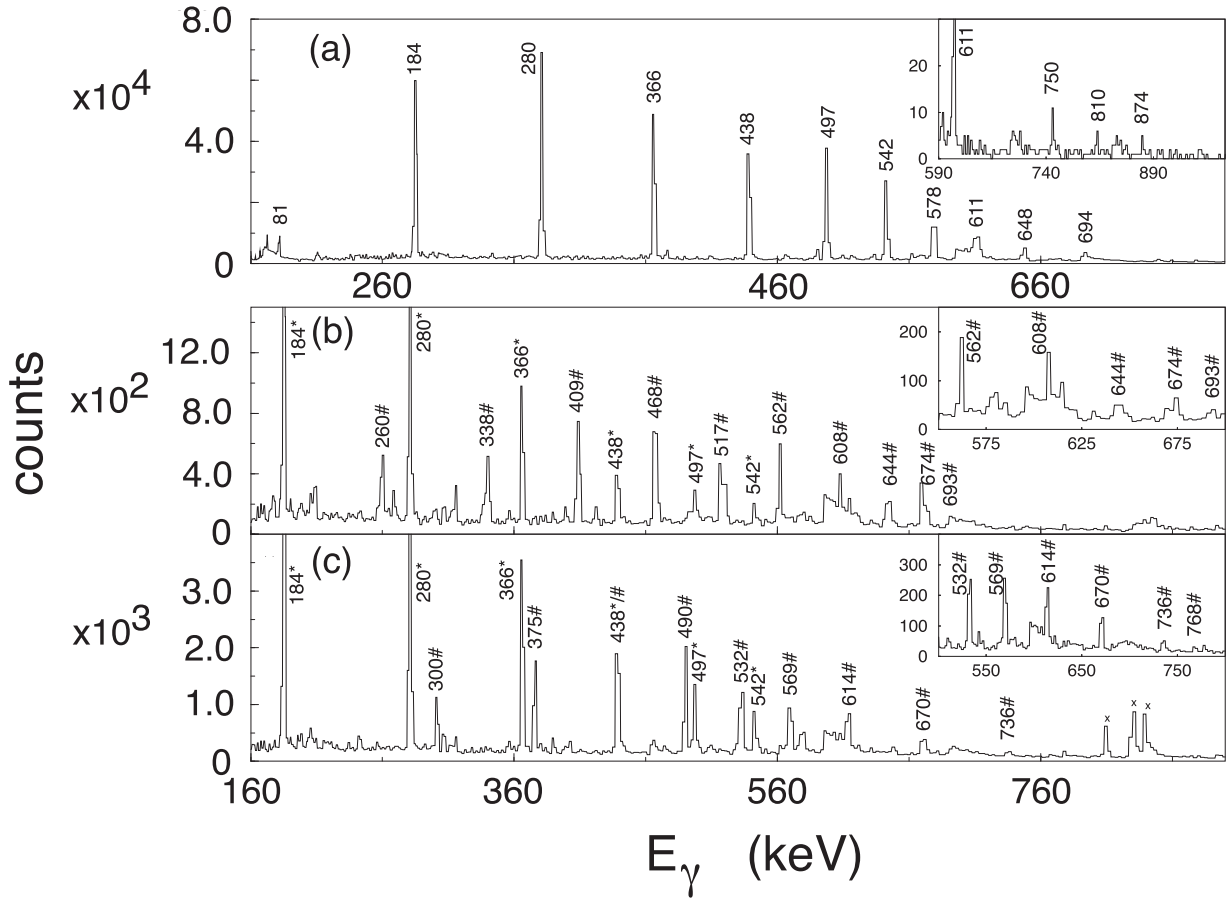


FIG. 7. Gamma-ray energy spectra corresponding to (a) the Yrast sequence in ^{166}Er, (b) the $\alpha = 0$ signature of the γ-vibrational band, and (c) the $\alpha = 1$ signature of the γ-vibrational band. See text for details of gating conditions. In spectra (b) and (c), the symbol # indicates transitions within the $\alpha = 0$ and $\alpha = 1$ signatures of the band, respectively. The symbol * in spectra (b) and (c) indicates transitions within the ground-state band.

and $\alpha = 1$) of ^{166}Er and the relative γ-ray intensities for interband transitions from the γ band ($\alpha = 0$ and $\alpha = 1$) to the ground-state band.

3. The $K^\pi = (0^+)$ band

The 1460-keV and 1528-keV levels of the $K^\pi = (0^+)$ band were first observed in ^{166}Ho β^- decay and in ^{166}Tm electron capture [27]. The assignment of these levels to a $K^\pi = (0^+)$ band and the extension to spin $12\hbar$ were made by Fields *et al.* [19]. In the present work, the crossing transitions from the 4^+, 6^+, 8^+, 10^+, and 12^+ states to the ground-state band (corresponding to γ-ray energies of 1409, 1352, 1283, 1130, and 809 keV, respectively) were identified, in agreement with the work of Fields *et al*. However, the states are very weakly populated and, in the present work, no new transitions were observed. Consequently, no γ-ray spectra are presented here.

4. The $K^\pi = (2^-, 5^-)$ band

Gamma rays of energies 1081, 1181, and 1417 keV have been identified as decaying from levels at 1992 (7^-), 2092 (7^-), and 2328 keV (9^-), respectively, to the 8^+ member of the ground-state band. The transitions correspond to the deexcitation of levels in the $K^\pi = (2^-, 5^-)$ structure established by Fields *et al.* [19]. The 7^- level at 1992 keV also decays to the 6^+ state of the ground-state band via a 1447-keV transition. The states were very weakly populated in the present work; only three of the seven levels observed by Fields *et al.* were identified. Consequently, no γ-ray spectra are presented here.

D. ^{167}Er

Figure 8 presents the level scheme for ^{167}Er from the present work. Only the ground-state band ($7/2^+[633]$) and the decay sequence based on the $1/2^-[521]$ configuration were populated with any significant strength. The γ-ray transitions in ^{167}Er were ordered according to the relative intensities shown in Table IV. Relative intensities and spin assignments for both bands populated and their corresponding interband transitions are shown. For previously known states, the I^π assignments of Fig. 8 and of Table IV are those of the recent Nuclear Data Sheets evaluation of Singh and Chen [28].

1. Ground-state band ($7/2^+[633]$)

Figure 9(a) shows a γ-ray spectrum resulting from the sum of all double gates involving the γ-ray transitions at energies of 178, 257, 338, 422, and 504 keV. The spectrum corresponds to the $\alpha = -\frac{1}{2}$ signature of the ground-state band; two new

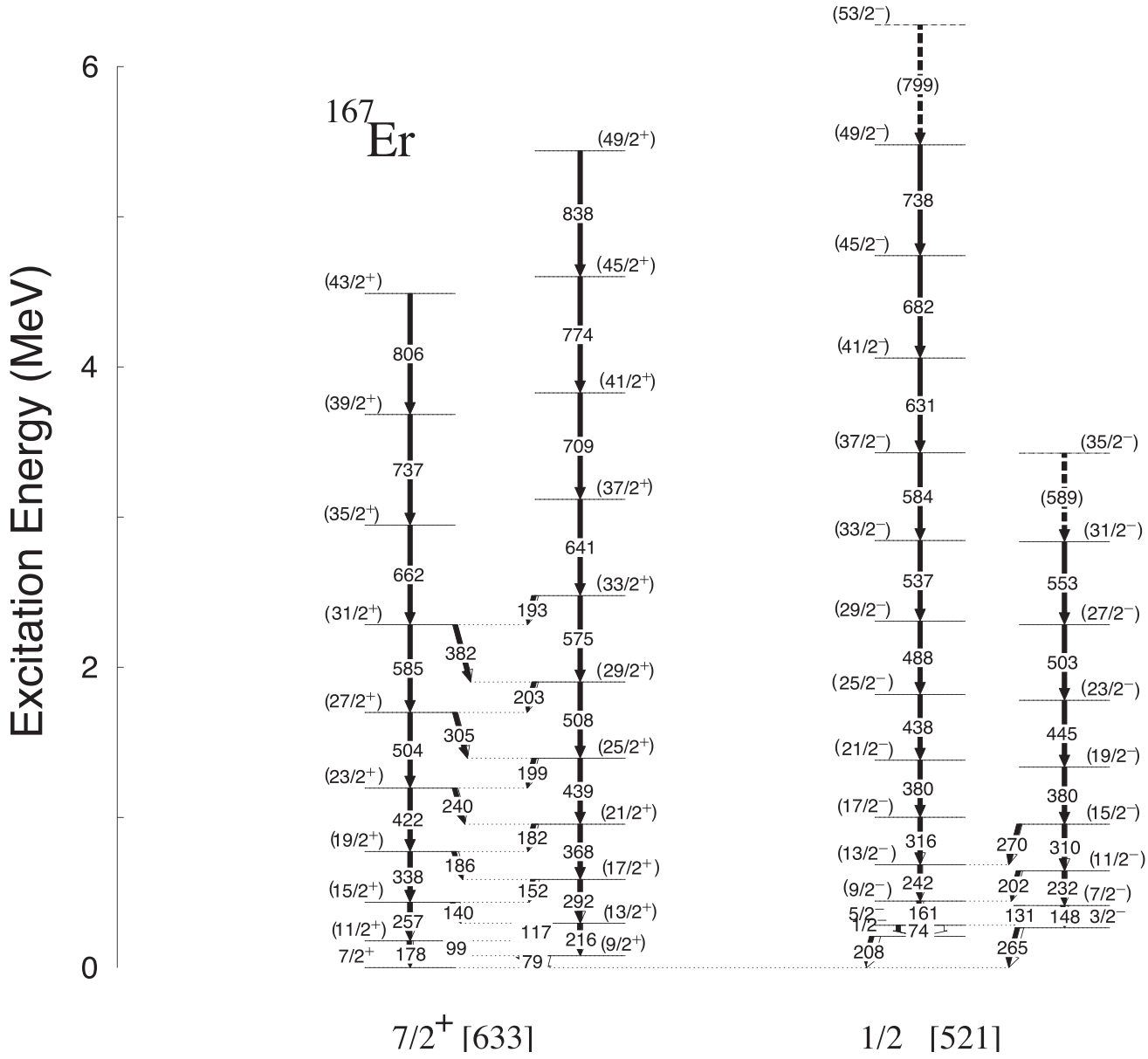


FIG. 8. Level scheme of ^{167}Er from the present work.

transitions (737 and 806 keV) have been added to the previous work of Gervais *et al.* [25], increasing the known spin from $(35/2^+)$ to $(43/2^+)$. The inset shows a partial γ-ray spectrum resulting from a double gate on the 504- and 662-keV transitions and shows evidence for the addition of the two new transitions at 737 ($(39/2^+) \rightarrow (35/2^+)$) and 806 keV ($(43/2^+) \rightarrow (39/2^+)$). It was not possible to measure the intensity of the γ-ray transition at 504 keV, since all individual or double gates resulted in a broad double peak. This was due to the presence of the $(29/2^+) \rightarrow (25/2^+)$ transition at 508 keV in the signature partner. The relative intensities of transitions in the two signatures of the band were normalized relative to the most intense photopeak measured, namely, the $(21/2^+) \rightarrow (17/2^+)$ (368-keV) transition in the $\alpha = +\frac{1}{2}$ signature of the band.

A γ-ray energy spectrum corresponding to the $\alpha = +\frac{1}{2}$ signature of the ground-state band is presented in Fig. 9(b). The spectrum shown is the result of a sum of all double gates on the 216-, 292-, 508-, and 641-keV transitions. Three new transitions have been added to the work of Gervais *et al.* [25] at γ-ray energies of 709, 774, and 838 keV. The inset to Fig. 9(b) shows a partial γ-ray spectrum resulting from a double gate on the 508- and 641-keV transitions; the extensions to the band can clearly be seen, resulting in an increase in the highest spin of the band to $(49/2^+)$.

2. *The* $1/2^-[521]$ *rotational sequence*

Figure 10 shows an example of a γ-ray spectrum corresponding to gates set on transitions within the $\alpha = +\frac{1}{2}$

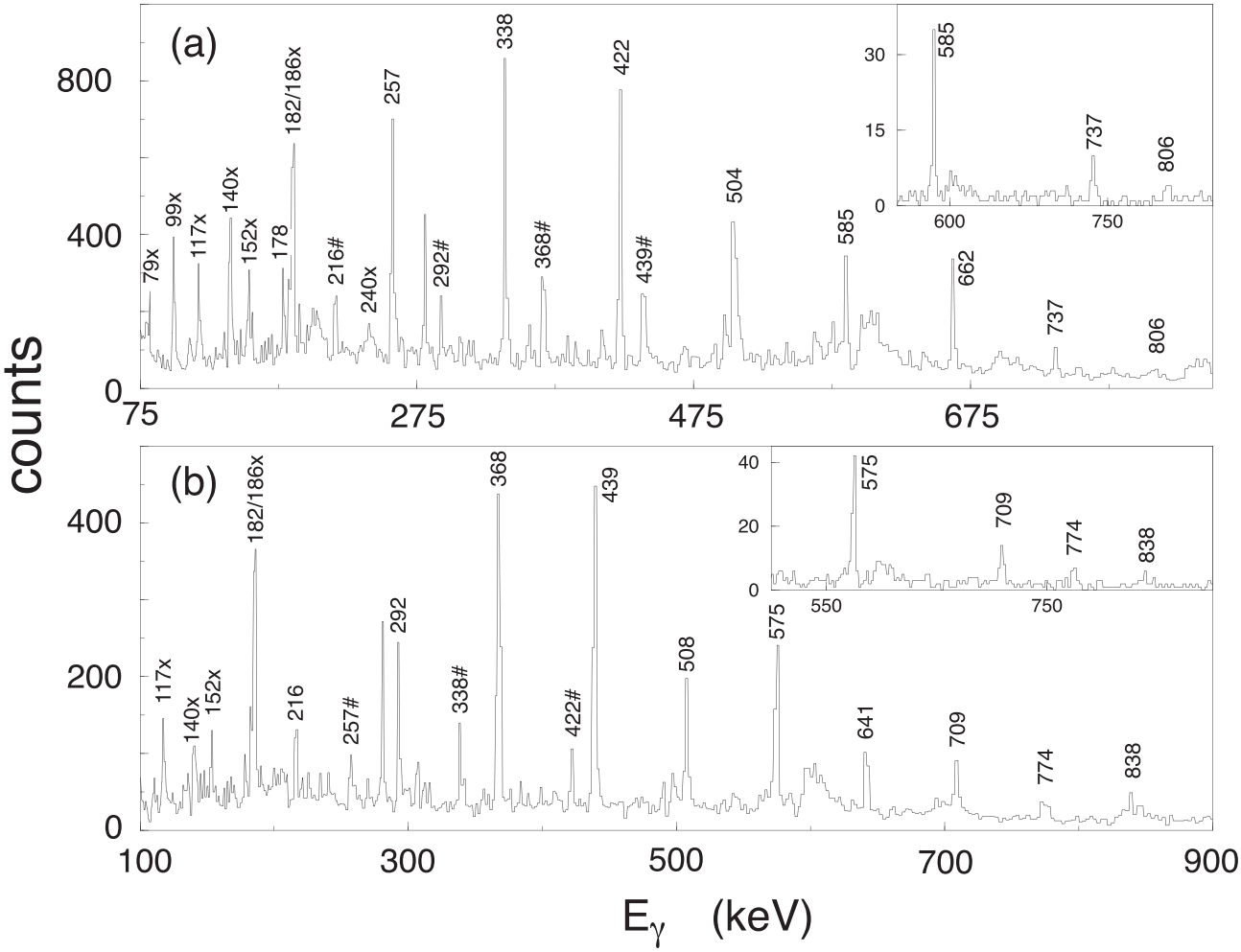


FIG. 9. Gamma-ray energy spectra corresponding to the (a) $\alpha = -\frac{1}{2}$ and (b) $\alpha = \frac{1}{2}$ signatures of the ground-state band in ^{167}Er. The peaks marked "x" are the $\Delta I = 1$ interband transitions, and those marked "#" are the in-band transitions in the signature partner. See text for the gating conditions.

signature of the $1/2^-[521]$ rotational sequence. The spectrum is the result of a sum of all double gates set on the photopeaks of energy 74, 161, 242, 316, 488, 537, 584, and 631 keV. Confirmation of the published level scheme and evidence for the proposed extensions to the band were based on such spectra. The rotational sequence based on the $\alpha = +\frac{1}{2}$ signature of the $1/2^-[521]$ single-neutron configuration was extended by three new transitions of energies 631, 682, and 738 keV, resulting from the deexcitation of states with spins $(41/2^-)$, $(45/2^-)$, and $(49/2^-)$, respectively. A fourth transition was also tentatively placed at 799 keV, corresponding to the decay of the $(53/2^-)$ state (see inset to Fig. 10). As a consequence of the large signature splitting, the unfavored signature partner of the band was very weakly populated. Figure 11 shows the γ-ray spectrum corresponding to a double gate set on transitions of energy 232 and 310 keV within the $\alpha = +\frac{1}{2}$ signature of the band. The inset, a partial spectrum, corresponds to a double gate set on transitions of energy 380 and 503 keV. Transitions depopulating states with spin up to $(31/2^-)$ can be seen (553-keV transition). A new addition to the band was tentatively identified at 589 keV, corresponding to the decay of a state with a proposed spin of $(35/2^-)$.

As the ^{167}Er channel was weakly populated, the interband transitions between two signatures of the $1/2^-[521]$ configuration were not sufficiently intense to normalize both signatures relative to each other. In addition to this, the interband transitions to the ground-state band were not of sufficient intensity to normalize the intensities relative to the ground-state band. Therefore, both signatures of the $1/2^-[521]$ configuration have been individually normalized and are presented separately in Table IV.

IV. DISCUSSION

The experimental Routhians and quasiparticle alignment plots discussed here show evidence for configuration-dependent band-crossing frequencies, quasiparticle blocking effects, and signature splitting. The cranked shell model [29] (CSM) has been used to interpret the experimental Routhians and alignments. The model is based on a modified harmonic

TABLE III. Relative γ-ray intensities for transitions in the γ-vibrational band ($\alpha = 0$ and $\alpha = 1$) of ^{166}Er and for interband transitions from the γ band ($\alpha = 0$ and $\alpha = 1$) to the ground-state band of ^{166}Er. See text for details.

E_γ (keV)	I_i^π	I_f^π	Relative intensity
170	4^+	2^+	
260	6^+	4^+	
338	8^+	6^+	114(4)
409	10^+	8^+	78(2)
468	(12^+)	10^+	58(2)
517	(14^+)	(12^+)	43(2)
562	(16^+)	(14^+)	29(4)
608	(18^+)	(16^+)	25(4)
644	(20^+)	(18^+)	25(4)
(674)	(22^+)	(20^+)	13(3)
(693)	(24^+)	(22^+)	11(2)
215	5^+	3^+	
300	7^+	5^+	127(5)
375	9^+	7^+	87(2)
438	(11^+)	9^+	86(5)
490	(13^+)	(11^+)	30(4)
532	(15^+)	(13^+)	19(3)
569	(17^+)	(15^+)	8.6(9)
614	(19^+)	(17^+)	5.1(7)
670	(21^+)	(19^+)	1.0(2)
736	(23^+)	(21^+)	0.5(2)
(768)	(25^+)	(23^+)	0.2(1)
670	6^+	6^+	41(2)
950	6^+	4^+	21.0(5)
1008	8^+	6^+	30(2)
1051	10^+	8^+	10.6(8)
1080	(12^+)	10^+	4.0(6)
401	9^+	10^+	3.2(5)
464	7^+	8^+	37(1)
595	3^+	4^+	17(6)
810	5^+	4^+	47(2)
822	(15^+)	14^+	0.7(2)
830	7^+	6^+	83(2)
832	(13^+)	12^+	95(8)
839	(11^+)	10^+	44(1)
839	9^+	8^+	95(2)

oscillator potential with a standard Nilsson parameter set. For ^{166}Er, the values of the deformation parameters ($\epsilon_2 = 0.266$ and $\epsilon_4 = 0.012$) were taken from the Lund systematics [30]. The neutron pairing gap parameter ($\Delta_n = 0.773$ MeV) was calculated using the formula of Bohr and Mottelson [31], using mass values taken from Ref. [32]. To approximate the effects of rotation on the pairing gap, the value of Δ_n was reduced to 80% of the calculated value. The results of CSM calculations for positive-parity quasineutron levels in ^{166}Er indicate that the ground-state band is crossed by the more energetically favored Stockholm band at $\hbar\omega = 265(10)$ keV; this AB band crossing corresponds in the present case to the alignment of a pair of $i_{13/2}$ quasineutrons. An AB alignment gain of $7.0\hbar$ is predicted by the CSM calculations and this is in good agreement with the experimental value of $7.1(1)\hbar$ for the

TABLE IV. Relative γ-ray intensities and spin assignments of all transitions populated in the $7/2^+[633]$ ground-state band and the $1/2^-[521]$ band of ^{167}Er. See text for details.

E_γ (keV) $7/2^+[631]$	I_i^π	I_f^π	Relative intensity
216	$(13/2^+)$	$(9/2^+)$	
292	$(17/2^+)$	$(13/2^+)$	
368	$(21/2^+)$	$(17/2^+)$	1000(50)
439	$(25/2^+)$	$(21/2^+)$	677(44)
508	$(29/2^+)$	$(25/2^+)$	409(22)
575	$(33/2^+)$	$(29/2^+)$	183(14)
641	$(37/2^+)$	$(33/2^+)$	120(13)
709	$(41/2^+)$	$(37/2^+)$	55(7)
774	$(45/2^+)$	$(41/2^+)$	14(4)
838	$(49/2^+)$	$(45/2^+)$	6(1)
178	$(11/2^+)$	$7/2^+$	
257	$(15/2^+)$	$(11/2^+)$	
338	$(19/2^+)$	$(15/2^+)$	663(50)
422	$(23/2^+)$	$(19/2^+)$	390(17)
504	$(27/2^+)$	$(23/2^+)$	x
585	$(31/2^+)$	$(27/2^+)$	234(12)
662	$(35/2^+)$	$(31/2^+)$	111(9)
737	$(39/2^+)$	$(35/2^+)$	51(7)
806	$(43/2^+)$	$(39/2^+)$	18(4)
79	$(9/2^+)$	$7/2^+$	
99	$(11/2^+)$	$(9/2^+)$	
117	$(13/2^+)$	$(11/2^+)$	
140	$(15/2^+)$	$(13/2^+)$	
152	$(17/2^+)$	$(15/2^+)$	240(39)
186	$(19/2^+)$	$(17/2^+)$	376(32)
182	$(21/2^+)$	$(19/2^+)$	81(11)
240	$(23/2^+)$	$(21/2^+)$	68(8)
199	$(25/2^+)$	$(23/2^+)$	59(9)
305	$(27/2^+)$	$(25/2^+)$	58(11)
203	$(29/2^+)$	$(27/2^+)$	15(4)
382	$(31/2^+)$	$(29/2^+)$	6(3)
193	$(33/2^+)$	$(31/2^+)$	17(4)
$1/2^-[521]$			
74	$5/2^-$	$1/2^-$	
161	$(9/2^-)$	$5/2^-$	
242	$(13/2^-)$	$(9/2^-)$	1000(113)
316	$(17/2^-)$	$(13/2^-)$	950(35)
380	$(21/2^-)$	$(17/2^-)$	875(33)
438	$(25/2^-)$	$(21/2^-)$	654(29)
488	$(29/2^-)$	$(25/2^-)$	517(27)
537	$(33/2^-)$	$(29/2^-)$	323(24)
584	$(37/2^-)$	$(33/2^-)$	179(21)
631	$(41/2^-)$	$(37/2^-)$	88(14)
682	$(45/2^-)$	$(41/2^-)$	65(9)
738	$(49/2^-)$	$(45/2^-)$	17(3)
(799)	$(53/2^-)$	$(49/2^-)$	6(3)
148	$(7/2^-)$	$3/2^-$	
232	$(11/2^-)$	$(7/2^-)$	
310	$(15/2^-)$	$(11/2^-)$	1000(13)
380	$(19/2^-)$	$(15/2^-)$	497(34)
445	$(23/2^-)$	$(19/2^-)$	352(43)
503	$(27/2^-)$	$(23/2^-)$	186(31)
553	$(31/2^-)$	$(27/2^-)$	128(26)
(589)	$(35/2^-)$	$(31/2^-)$	58(8)

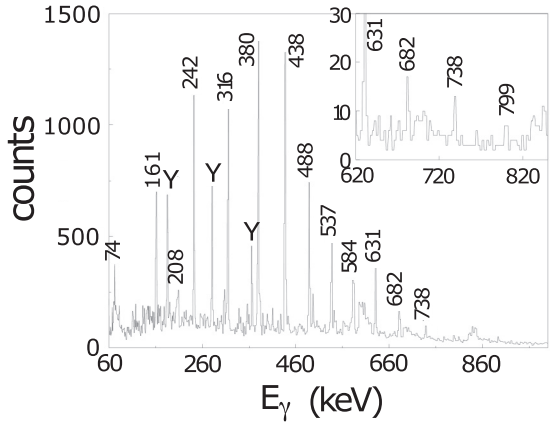


FIG. 10. Gamma-ray energy spectra corresponding to transitions within the $\alpha = +\frac{1}{2}$ signature of the $1/2^-[521]$ rotational sequence in ^{167}Er. The spectrum is the result of a sum of all double gates set on the photopeaks of energy 74, 161, 242, 316, 488, 537, 584, and 631 keV. The peaks marked "Y" correspond to the yrast decay sequence of ^{166}Er, brought in by the gating. The inset corresponds to the partial spectrum resulting from a double gate on the 508- and 641-keV transitions.

yrast sequence. Higher crossings take place at 0.26 MeV (A $\rightarrow$ ABC) and 0.39 MeV (B $\rightarrow$ BAD), with alignment gains of 6.6(2)$\hbar$ and 0.39(2)$\hbar$, respectively.

A. ^{165}Er

Experimental quasiparticle Routhians and aligned angular momenta plotted as a function of rotational frequency are

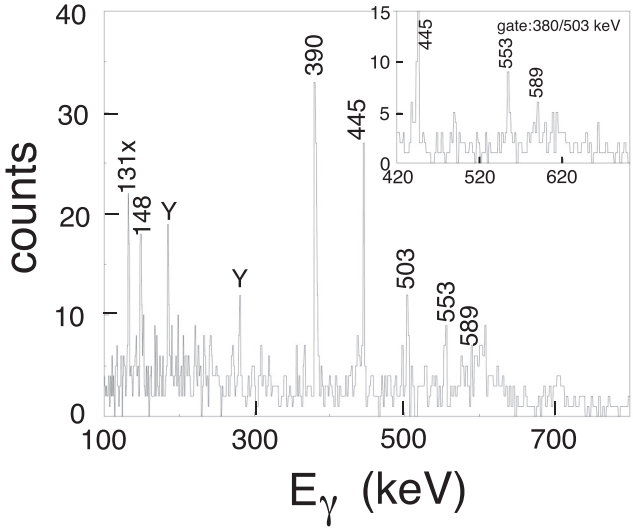


FIG. 11. Gamma-ray energy spectra corresponding to transitions within the $\alpha = -\frac{1}{2}$ signature of the $1/2^-[521]$ rotational sequence in ^{167}Er. The spectrum is the result of a double gate set on the photopeaks of energy 232 and 310 keV. The peaks marked "Y" correspond to the yrast decay sequence of ^{166}Er, brought in by the gating. The inset corresponds to the partial spectrum resulting from a double gate on the 380- and 503-keV transitions.

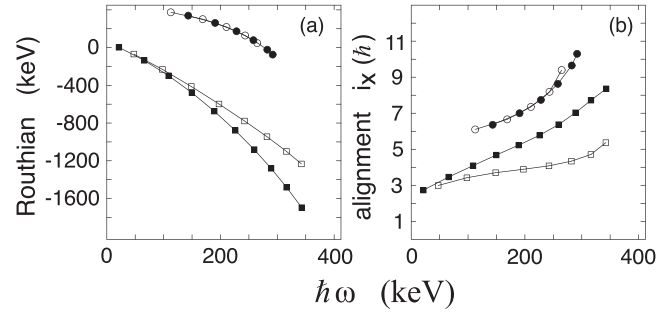


FIG. 12. (a) Experimental Routhians and (b) quasiparticle alignments plotted as a function of rotational frequency for ^{165}Er. The plots show rotational sequences based on the $11/2^-[505]$ (circles) and $5/2^+[642]$ (squares) Nilsson configurations; the solid (open) symbols represent the $\alpha = +\frac{1}{2}$ ($-\frac{1}{2}$) signature of the bands. The quasiparticle alignment of the $11/2^-[505]$ rotational sequence has been offset by 5$\hbar$ for clarity of presentation.

presented in Fig. 12 for the bands populated in ^{165}Er. A reference band has been subtracted with Harris parameters $J^0 = 32.8\hbar^2\,\text{MeV}^{-1}$ and $J^1 = 56.9\hbar^4\,\text{MeV}^{-3}$. The Harris parameters were obtained by fits to the low-spin (zero-quasiparticle) members of the yrast sequences of ^{164}Er, ^{166}Er, and ^{168}Er. Values for the odd-A isotopes, ^{165}Er and ^{167}Er, were obtained by interpolation.

1. The $11/2^-[505]$ *band*

The $11/2^-[505]$ band is represented by circles in Fig. 12. The experimental Routhians, Fig. 12(a), show a gradual crossing between the one- and the three-quasiparticle bands, corresponding to the alignment of a pair of $i_{13/2}$ quasineutrons. Due to the strong interaction between the one- and three-quasiparticle states, the transition to the aligned two-quasiparticle regime is very smooth. It would appear that, in the rotational frequency range populated, the full alignment gain has not been observed [see Fig. 12(b)]. The two signatures of the band appear to undergo approximately the same gradual gain in alignment, with the $\alpha = +\frac{1}{2}$ signature gaining 3.9$\hbar$ and the $\alpha = -\frac{1}{2}$ signature gaining 3.4$\hbar$ over the observed frequency range. The experimental full alignment gain in the ground-state yrast band of the even-even core, ^{164}Er [33], is $\approx$7$\hbar$; here the observed alignment gain is just over half of the full value. The frequency of the alignment of the $i_{13/2}$ neutron pair is sensitive to the pairing energy, which is configuration dependent when higher multipole terms are included [34,35]. The $11/2^-[505]$ orbital is strongly oblate and therefore has little overlap with the aligning high-j low-Ω prolate $i_{13/2}$ orbitals. Consequently, the occupation of the $11/2^-[505]$ orbital has little effect on the frequency at which the $i_{13/2}$ neutrons align. The first crossing frequency in the $11/2^-[505]$ band is therefore expected to be similar to that of the even-even core, ^{164}Er, namely, 267(2) keV [33]. This effect was first discussed by Garrett *et al.* [36]. In the absence of the observation of full alignment gain, it is difficult to draw definitive conclusions in relation to the crossing frequency; however, it is noted that the frequency corresponding to half of the observed alignment gain ($\approx$270 keV) agrees with that

of the even-even core. The absence of signature splitting is also noted; this is a consequence of the large Ω value of the bandhead.

2. The $5/2^+[642]$ *band*

The $5/2^+[642]$ Nilsson configuration originates from the $i_{13/2}$ spherical shell-model state. It therefore blocks the $i_{13/2}$ AB alignment and the alignment of the BC and AD quasineutrons will be observed at a higher rotational frequency than the AB alignment in the even-even ^{164}Er core (267(2) keV [33]). The $\alpha = -\frac{1}{2}$ signature branch appears to show an upbend at a frequency of 350 keV [Fig. 12(b)], and this is confirmed in the work of Wang *et al.* [14], where the band is extended to a higher frequency. This corresponds to the alignment of an AD neutron pair. Within the context of the cranked shell model, as noted above, the AD crossing takes place at a frequency of 0.39 MeV, which is not inconsistent with the observation of an upbend near 350 keV. In ^{159}Er, for comparison, the yrast band at low frequencies is the quasineutron configuration A and corresponds to the favored ($\alpha = +\frac{1}{2}$) signature originating from the $3/2^+[651]i_{13/2}$ Nilsson state. This configuration is crossed at a frequency of 360 keV by the three-quasineutron configuration ABC in which a pair of $i_{13/2}$ neutrons (BC) have aligned [37]. The unfavored signature of the $3/2^+[651]$ configuration is observed to upbend at approximately the same rotational frequency as in the yrast band (≈360 keV); this is due to the alignment of the pair of $i_{13/2}$ neutrons AD. The experimental Routhians, Fig. 12(a), show an increasingly large signature splitting with increasing rotational frequency; this is due to an increasingly large $K = 1/2$ component in the wave function of the rotational sequence with increasing rotational frequency. Over the observed frequency range, the quasiparticle alignment gain (Δi_x) in the $\alpha = +\frac{1}{2}$ signature of the band is 5.5ħ, whereas, in the $\alpha = -\frac{1}{2}$ signature, the gain is 2.3ħ [Fig. 12(b)]. The large gain in alignment in the $\alpha = +\frac{1}{2}$ signature of the band is due to mixing with the strongly favored $\alpha = +\frac{1}{2}$ signature of the $K = 1/2$ component of the wave function.

B. ^{166}Er

Figure 13 shows the experimental Routhians and quasiparticle aligned angular momenta as a function of rotational frequency for the yrast and γ-vibrational decay sequences of ^{166}Er. A reference band has been subtracted with Harris parameters $J^0 = 35.0\hbar^2\,\mathrm{MeV}^{-1}$ and $J^1 = 60.0\hbar^4\,\mathrm{MeV}^{-3}$.

^{166}Er, with neutron number 98, is expected to exhibit a strong interaction between the ground-state band and the crossing band. As may be seen in Fig. 13, both the yrast and the γ-vibrational bands are observed to undergo a gradual gain in alignment with increasing rotational frequency. A gradual "upbend" is apparent rather than the sharp backbend seen in the case of weak interaction strength [see Fig. 13(b)].

The experimental Routhians, Fig. 13(a), show that, for the yrast sequence, the AB band crossing takes place at a rotational frequency of 267(2) keV. The gain in quasiparticle alignment is 7.1(1)ħ [see Fig. 13(b)]. The initial alignment of the γ-vibrational band is ≈0.5ħ and the band crosses

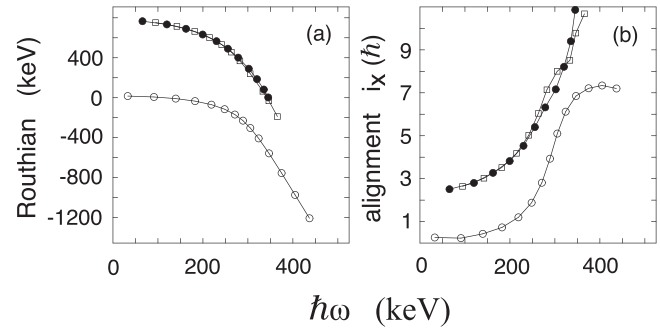


FIG. 13. (a) Experimental Routhians and (b) quasiparticle alignment plotted as a function of rotational frequency for ^{166}Er. The plot shows the Yrast sequence (open circles), and $\alpha = 0$ and 1 signatures of the γ-vibrational band (closed circles and open squares, respectively). The quasiparticle alignment of the γ band has been offset by 2ħ for the purposes of clarity of presentation.

the $i_{13/2}$ two-quasineutron band at a rotational frequency of 262(2) keV. The gain in quasiparticle alignment for the γ-vibrational band of 8.8(1)ħ is higher than we would expect for the alignment of two $i_{13/2}$ quasineutrons (7.0ħ); this may be a consequence of the tentative nature of the high-spin transitions.

As noted above, the results of CSM calculations for positive-parity quasineutron levels in ^{166}Er indicate that the ground-state band is crossed by the more energetically favored Stockholm band at $\hbar\omega = 265(10)$ keV; this AB band crossing corresponds in the present case to the alignment of a pair of $i_{13/2}$ quasineutrons. The CSM value of crossing frequency is in very good agreement with the experimental value of 267(2) keV for the yrast sequence. An AB alignment gain of 7.0ħ is predicted by the CSM calculations and this is in very good agreement with the experimental value of 7.1(1)ħ for the yrast sequence. Similarly, there is good agreement between experiment and the results of CSM calculations for the crossing frequency in the γ-vibrational band.

Earlier work [20] has investigated triaxiality in ^{166}Er through an almost complete set of reduced $E2$ matrix elements for the ground-state and γ bands up to spin 14^+ and 12^+, respectively. The data suggest that the collective structure of ^{166}Er can be understood in terms of a varying dynamic triaxiality from $\gamma \approx 18^\circ$ for the ground state to $\gamma \approx 10^\circ$ for the higher spin states of the ground-state band and for the γ band. The extension of these results to the higher-spin states populated in the present experiment would be very instructive. Whether the data of Fig. 13, in particular the lack of signature splitting in the Routhians, are consistent with a varying dynamic triaxiality, especially if it extends to higher spin states, is beyond the scope of the present paper.

C. ^{167}Er

Experimental Routhians and aligned angular momenta, plotted as a function of rotational frequency, are presented in Figs. 14 and 15 for the bands populated in ^{167}Er. A reference band has been subtracted with Harris parameters $J^0 = 37.2\hbar^2\,\mathrm{MeV}^{-1}$ and $J^1 = 63.1\hbar^4\,\mathrm{MeV}^{-3}$.

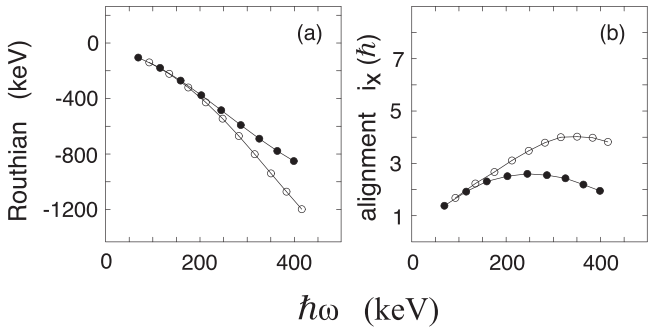


FIG. 14. (a) Experimental Routhians and (b) quasiparticle alignment plotted as a function of rotational frequency for the $7/2^+[633]$ ground-state configuration in ^{167}Er. The solid (open) symbols represent the $\alpha = -\frac{1}{2}$ ($\alpha = +\frac{1}{2}$) signature of the band.

1. The $7/2^+[633]$ *band*

The $7/2^+[633]$ configuration is based on the $i_{13/2}$ neutron spherical shell-model state. Its occupancy therefore blocks the AB alignment and the first crossing is delayed to a higher frequency than that observed in the yrast sequence of the ^{166}Er core nucleus. Based on the results of CSM calculations (see above), the first band crossing is expected to be observed at 0.32 MeV (A $\rightarrow$ BC) and at 0.39 MeV (B $\rightarrow$ AD). However, there is no clear evidence for the band crossing near these frequencies in the present data. The gain in alignment, Fig. 14(b), is unexpectedly small, especially for the $\alpha = -\frac{1}{2}$ signature of the band, and the alignment does not continue to increase with increasing rotational frequency. In cranked shell-model calculations, the BC and AD alignments are 6.6$\hbar$ and 4.4$\hbar$, respectively.

2. The $1/2^-[521]$ *band*

The experimental routhians, Fig. 15(a), for the $1/2^-[521]$ rotational sequence show a reasonably small signature splitting at low rotational frequencies. However, as the rotational frequency is increased, the splitting increases rapidly and this is consistent with the results of CSM calculations (see Ref. [38]). The rotational sequence can be seen to cross with the aligned $i_{13/2}$ two-quasineutron band at a rotational frequency

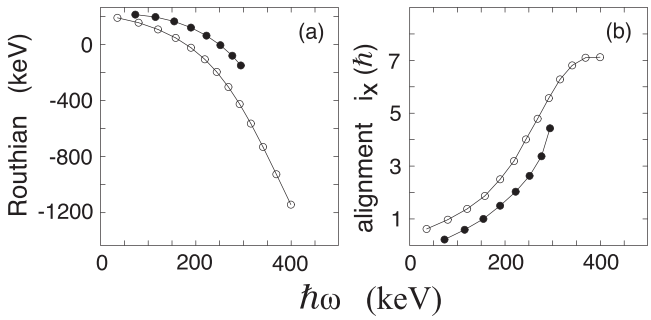


FIG. 15. (a) Experimental routhians and (b) quasiparticle alignment plotted as a function of rotational frequency for the $1/2^-[521]$ rotational sequence in ^{167}Er. The solid (open) symbols represent the $\alpha = -\frac{1}{2}$ ($\alpha = +\frac{1}{2}$) signature of the band.

of around 250(8) keV. The band-crossing frequency is reduced compared with the experimental value of 267(2) keV for the even-even ^{166}Er core. This is a consequence of the reduced pairing correlations caused by the blocking effect of the odd $p_{3/2}$ quasineutron. Over the frequency range populated, the observed gradual increase in quasiparticle alignment is, as noted earlier, a result of the proximity to a maximum in interaction strength at $N = 98$. The alignment gain of approximately 7$\hbar$ for the $\alpha = +\frac{1}{2}$ signature of the band is reproduced in cranked shell-model calculations (7.0$\hbar$). A constant spacing of $\approx$1$\hbar$ is also noted in the alignments of the two signatures of the rotational sequence.

D. Comparison with the results of the Projected Shell Model

The Projected Shell Model (PSM) [39] is a shell-model configuration mixing method that constructs its model basis from angular-momentum-projected multi-quasiparticle (qp) states. The model was established in the early 1990s by Hara and Sun aiming at describing rotational bands in well-deformed nuclei. In their first publications [40,41], the even-even isotope ^{166}Er and the odd neutron isotopes ^{165}Er and ^{167}Er were chosen as examples for the model demonstration. Among the early PSM works, it was shown [42] that the model can well describe the signature splitting effect in odd-mass nuclei. Later, the PSM was successfully applied to various isotopes to interpret high-spin rotational bands in deformed odd-proton nuclei (see Refs. [43–45], for example).

The PSM employs the Nilsson potential to generate deformed single-particle states. The pairing correlation is included through a BCS calculation. The violated angular momentum quantum number in the deformed quasiparticle states (both for protons and neutrons) is recovered by the angular-momentum-projection technique [46]. Therefore, in the PSM, the theoretical results can be compared level-to-level with experimental data (for example, those presented in Figs. 2, 6, and 8 of the present article), without the need for transforming the data to the Routhian frame. The original version of the PSM [39] adopted a deformed basis that maintains axial symmetry. This restriction was later released by introducing a triaxially deformed basis that includes both axial and triaxial deformations, described by the parameters ϵ_2 and ϵ' [47]. The so-called Triaxial Projected Shell Model (TPSM), which extends the PSM by performing a three-dimensional angular momentum projection, was shown to improve the capability of the model [46]. In addition to the usual ground-state rotational band, the TPSM can simultaneously describe the excited γ-vibrational band [48–50].

To generate realistic deformed single-particle states for ^{165,166,167}Er, we use the optimized Nilsson parameters in our recent publication [51]. The calculation employs the quadrupole deformation parameters $\epsilon_2 = 0.258$ and $\epsilon_2 = 0.267$ for the odd-neutron nuclei, ^{165}Er and ^{167}Er, respectively. The even-even ^{166}Er data include the rotational ground-state band and the γ-vibrational band. To describe this isotope, we perform TPSM calculations with axial deformation parameter $\epsilon_2 = 0.273$ and triaxial deformation parameter $\epsilon' = 0.130$. The monopole-pairing strength is parametrized as $G_M = [G_1 \mp G_2(N - Z)/A]/A$, where the minus sign applies

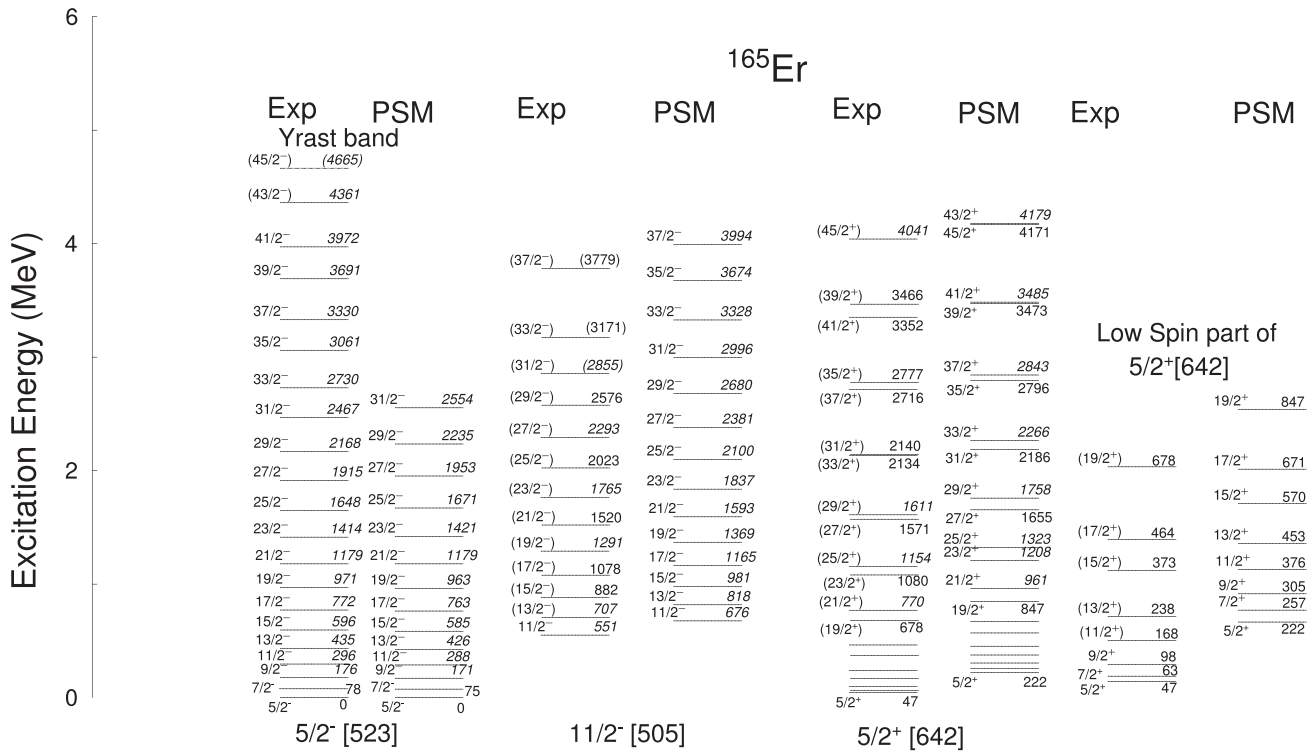


FIG. 16. Comparison of experimental and the calculated (PSM) level structures for ^{165}Er. For the $5/2^-[523]$ rotational sequence, the results of Wang *et al.* [14] have been included. See text for details.

to neutrons and the plus sign to protons, with $G_1 = 20.12$ and $G_2 = 13.13$. For the odd-neutron isotopes, we apply a 0.90 reduction factor for the neutron monopole-pairing strength, to account for the pairing attenuation induced by the unpaired neutron. The quadrupole-pairing strength G_Q is proportional to G_M with a fixed proportionality constant 0.16, consistent with the standard PSM parametrization for rare-earth nuclei [39].

In Figs. 16, 17, and 18, the PSM calculations are compared with the experimental data. Overall, the calculation successfully reproduces the characteristic features for the three isotopes up to the highest spin states observed. The root-mean-square deviation (RMSD) between experiment and theory over the complete spin range for all three isotopes is in the range from 120 to 180 keV. Remarkably, for the $5/2^-[523]$ rotational sequence in ^{165}Er, the RMSD is as small as 33 keV. For the γ-vibrational band of ^{166}Er, there is a good correspondence between experimental and theoretical excitation energies for spins less than 20^+; for higher spin values the theoretical signature splitting deviates significantly from the experimental values. If a comparison of experiment and theory is restricted to spins less than 20^+, the RMSD is significantly reduced from 137 to 50 keV.

Some of the rotational bands in the odd-neutron isotopes exhibit signature splitting manifested as zigzag patterns, such as the $5/2^+[642]$ band in ^{165}Er, and the $7/2^+[633]$ yrast band and $1/2^-[521]$ band in ^{167}Er. These oscillations follow the established signature splitting rule [41,42] where states with $I - j =$ even (odd) are energetically favored (unfavored), with I representing the total angular momentum and j denoting the spherical-limit angular momentum of the band's primary configurations.

In Fig. 16, the calculated rotational bands in ^{165}Er are plotted, and compared with the experimental data based on the present experiment together with that of Wang *et al.* [14] for the $5/2^-[523]$ rotational sequence. As one can see, our calculation for the $5/2^-[523]$ yrast band achieves excellent agreement with the experimental data. For the excited rotational bands assigned to $11/2^-[505]$ and $5/2^+[642]$ configurations, the calculation also shows remarkable consistency with experimental data. The distinct features of the two bands, that the high-K $11/2^-[505]$ band exhibits characteristic behavior without signature splitting, while the $5/2^+[642]$ configuration displays pronounced signature oscillations, are correctly obtained by the calculation. The latter configuration, originating from the neutron $1i_{13/2}$ orbital, follows the theoretically predicted signature splitting pattern where states with $I - 13/2 =$ even (corresponding to spins 5/2, 9/2, …) are energetically favored, in full accordance with the calculation.

In ^{167}Er, the calculation for the $7/2^+[633]$ ground-state configuration shows an excellent agreement with experimental data, displaying small-amplitude signature oscillations. This configuration, derived from the neutron $1i_{13/2}$ spherical orbital, adheres to the established signature splitting rule. The excited $1/2^-[521]$ band, constructed from the configuration with $K = 1/2$ originating from the $3p_{3/2}$ orbital, manifests a pronounced signature splitting effect. Our calculation accurately reproduces the observed pattern where states with $I - 3/2 =$ even (corresponding to spins 3/2, 7/2, 11/2, …) are energetically favored, although the theoretical energy curve

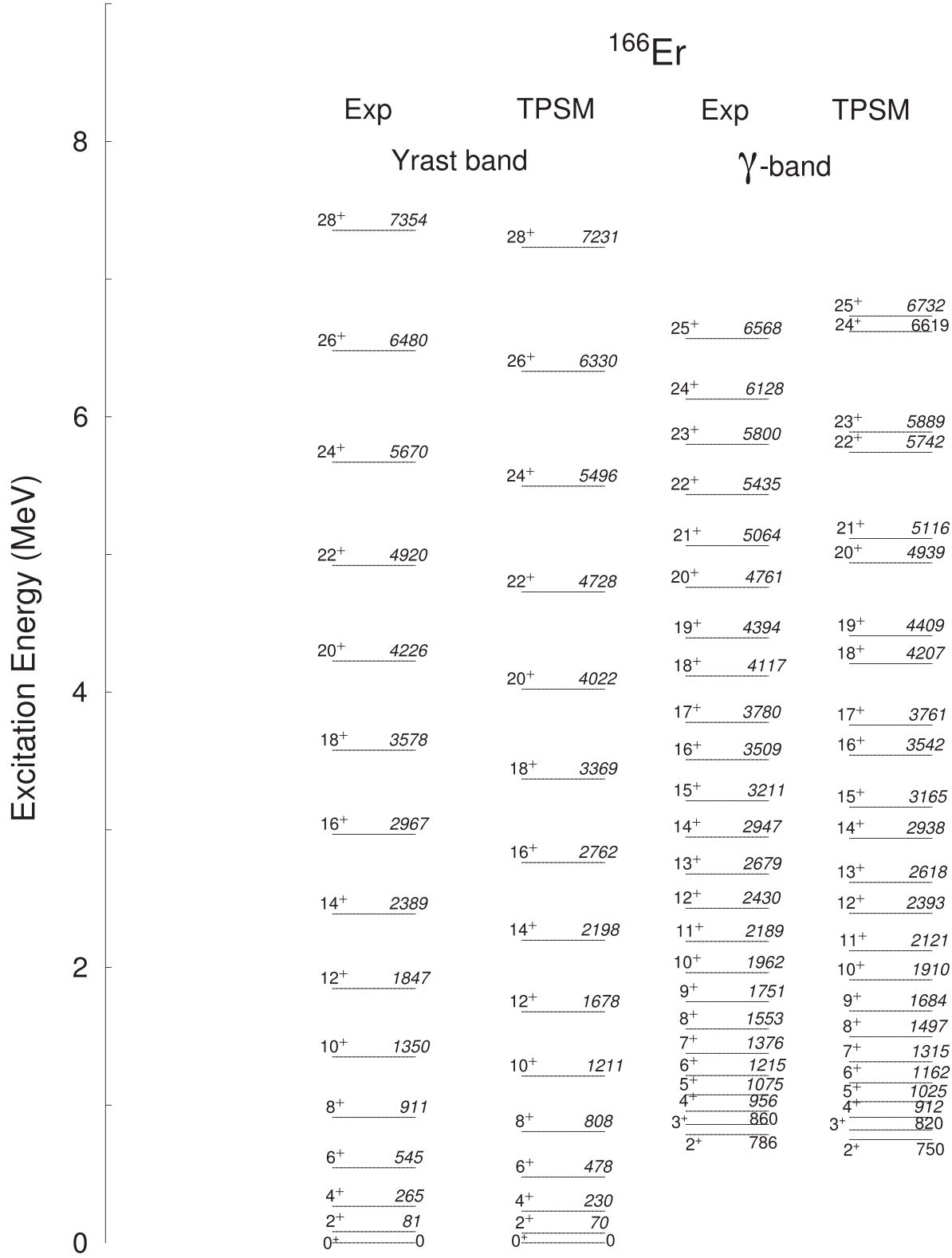


FIG. 17. Comparison of experimental and calculated (TPSM) level structures for ^{166}Er. See text for details.

shows a systematic upward shift relative to experimental data and exhibits enhanced signature splitting amplitude.

For the even-even isotope ^{166}Er, implementation of the TPSM calculations yields satisfactory results for both the ground-state band and γ-vibrational band, thus demonstrating an excellent description of experimental data. Especially for the entire rotational sequence of the γ band, from the bandhead 2^+ state up to all high spins below 20^+, good agreement between theoretical results and experimental data is evident.

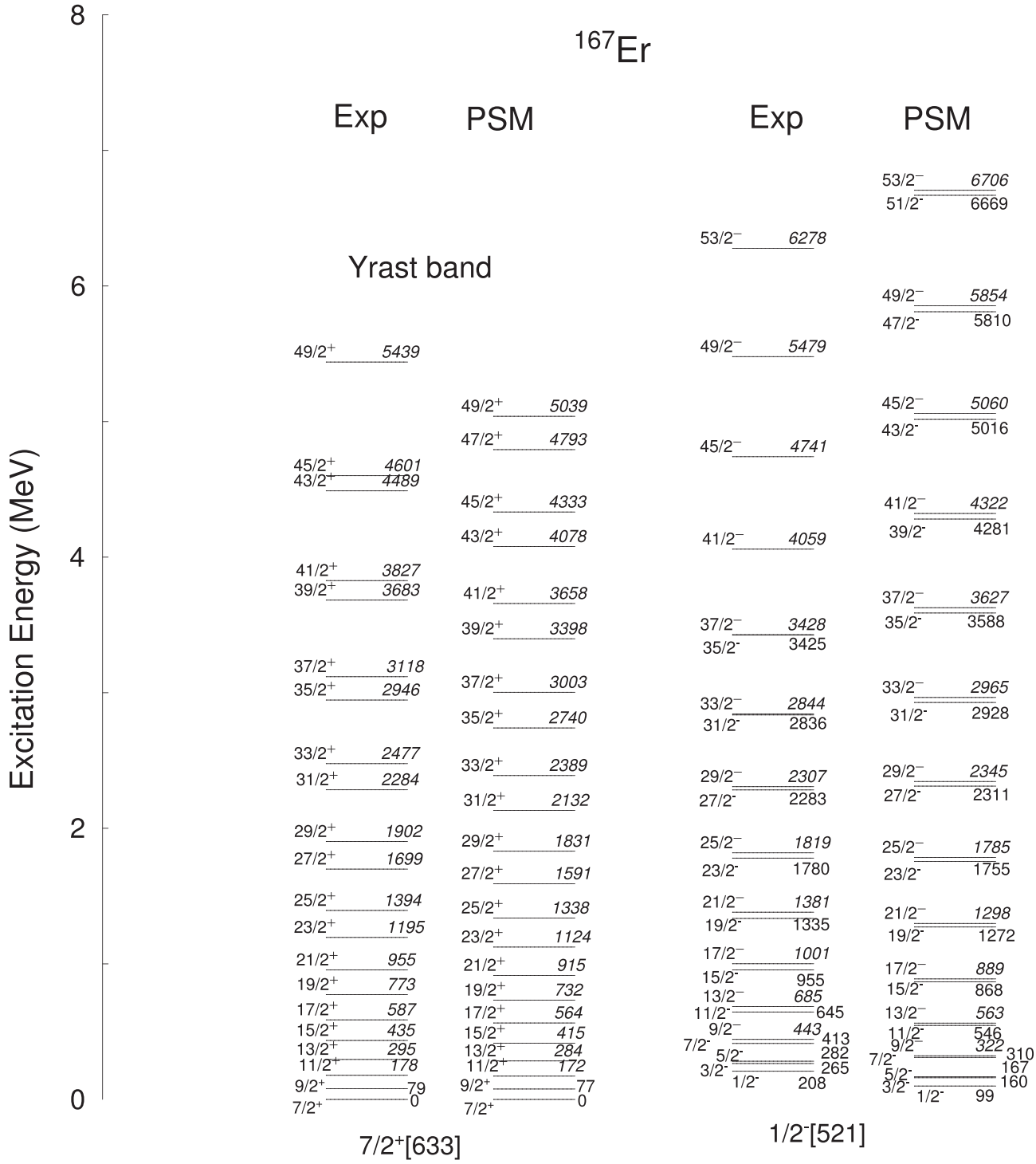


FIG. 18. Comparison of experimental and calculated (PSM) level structures for ^{167}Er. See text for details.

V. CONCLUSIONS

In this work, high-spin states of the erbium isotopes ^{165}Er, ^{166}Er, and ^{167}Er have been studied using incomplete fusion reactions initiated by a 55-MeV beam of ^{7}Li ions incident on a thin target of ^{164}Dy. The light p, d, and t ejectiles were detected using the ISIS ΔE-E silicon array and coincident γ rays were detected using the GASP array of escape-suppressed Ge detectors. Rotational states of ^{165}Er, ^{166}Er, and ^{167}Er were observed to spins $(45/2^+)$, (28^+), and $(53/2^-)$, respectively. The experimental Routhians and quasiparticle alignment plots discussed here show evidence for configuration-dependent band-crossing frequencies, quasiparticle blocking effects,

and signature splitting. For the nuclei studied here, around $N = 98$, there is expected to be an absence of sharp backbends, and this is consistent with observation. Alignment gains and crossing frequencies in the populated rotational sequencies were compared with the results of the Cranked Shell Model with standard parameters.

Projected Shell Model calculations performed here successfully reproduce the characteristic features of the three isotopes up to the highest spin states observed; excitation energies are overall well reproduced. The observed signature splitting in the odd-neutron isotopes in rotational sequences, such as the $5/2^+[642]$ band in ^{165}Er and the $7/2^+[633]$ yrast band in ^{167}Er, is accurately reproduced in the calculations, as is the lack of signature splitting in the high-K $11/2^-[505]$ band. Similarly, the pronounced signature splitting of the $1/2^-[521]$ band of ^{167}Er is accurately reproduced. For the ^{166}Er even-even isotope, the implementation of the Triaxial Projected Shell Model has yielded satisfactory results for both the ground-state band and the γ-vibrational band. Indeed, especially for the entire rotational sequence of the γ band, from the 2^+ bandhead state to all high spins below 20^+, a one-to-one correspondence between theoretical and experimental results is evident.

ACKNOWLEDGMENTS

We would like to thank the technical staff of the INFN Legnaro National Laboratory for their support during this experiment. This work was supported by the EPSRC (UK). Three of us (M.J.B., J.O., and M.L.) would like to acknowledge the receipt of financial support from EPSRC during the course of this work. The theoretical work is supported by the Special Foundation for Theoretical Physics, National Natural Science Foundation of China (NSFC), Grant No. 12347125, by China Postdoctoral Science Foundation, Grants No. 2023TQ0217 and No. 2024M751951, and by NSFC Grant No. 12235003.

DATA AVAILABILITY

The data that support the findings of this article are not publicly available. The data are available from the authors upon reasonable request.

[1] T. Otsuka, A. Gade, O. Sorlin, T. Suzuki, and Y. Utsuno, Rev. Mod. Phys. **92**, 015002 (2020).
[2] J. Dobaczewski, I. Hamamoto, W. Nazarewicz, and J. A. Sheikh, Phys. Rev. Lett. **72**, 981 (1994).
[3] J. Ollier, J. Simpson, M. A. Riley, E. S. Paul, X. Wang, A. Aguilar, M. P. Carpenter, I. G. Darby, D. J. Hartley, R. V. F. Janssens, F. G. Kondev, T. Lauritsen, P. J. Nolan, M. Petri, J. M. Rees, S. V. Rigby, C. Teal, J. Thomson, C. Unsworth, S. Zhu *et al.* Phys. Rev. C **83**, 044309 (2011).
[4] A. J. Hartley, R. Chapman, G. D. Dracoulis, S. Flanagan, W. Gelletly, and J. N. Mo, J. Phys. A **6**, L60 (1973).
[5] A. Faessler, F. Grümmer, L. Lin, and J. Urbano, Phys. Lett. B **48**, 87 (1974).
[6] D. Bazzacco *et al.*, in *Proceedings of the Conference on Nuclear Structure at High Angular Momentum, Ottawa* (AECL, Ottawa, 1992), p. 10613.
[7] C. R. Alvarez, Nucl. Phys. News **3**, 10 (1993).
[8] E. Farnea, G. de Angelis, M. De Poli, D. De Acuña, A. Gadea, D. R. Napoli, P. Spolaore, A. Buscemi, R. Zanon, R. Isocrate, D. Bazzacco, C. Rossi Alvarez, P. Pavan, A. M. Bizzeti-Sona, and P. G. Bizzeti, Nucl. Instrum. Methods Phys. Res., Sect. A **400**, 87 (1997).
[9] A. G. Smith (private communication).
[10] D. C. Radford, Nucl. Instrum. Methods Phys. Res., Sect. A **361**, 297 (1995).
[11] P. O. Tjøm and B. Elbek, Mat. Fys. Medd. Dan. Vid. Selsk **37**, no. 7 (1969).
[12] S. A. Hjorth, H. Ryde, K. A. Hagemann, G. Løvhøiden, and J. C. Waddington, Nucl. Phys. A **144**, 513 (1970).
[13] W. Andrejtscheff, P. Manfrass, H. Prade, K. D. Schilling, G. Winter, H. Fuia, R. Ion-Mihai, A. B. Khalikulov, V. A. Morozov, N. Z. Marupov, and T. M. Muminov, Nucl. Phys. A **220**, 438 (1974).
[14] S. T. Wang, X. H. Zhou, Y. H. Zhang, Y. Zheng, M. L. Liu, L. Chen, N. T. Zhang, W. Hua, S. Guo, Y. H. Qiang, G. S. Li, B. Ding, Y. Shi, and F. R. Xu, Phys. Rev. C **84**, 017303 (2011).
[15] S. T. Wang, X. H. Zhou, Y. H. Zhang, Z. Y. Sun, Y. Zheng, M. L. Liu, L. Chen, N. T. Zhang, J. Hu, F. Ma, W. Hua, S. Guo, Y. H. Qiang, L. Ma, Y. D. Fang, G. S. Li, H. B. Zhou, B. Ding, H. X. Wang, X. G. Lei *et al.* Phys. Rev. C **84**, 037303 (2011).
[16] T. P. D. Swan, P. M. Walker, Zs. Podolyák, M. W. Reed, G. D. Dracoulis, G. J. Lane, T. Kibédi, and M. L. Smith, Phys. Rev. C **85**, 024313 (2012).
[17] W. F. Davidson, R. M. Lieder, H. Beuscher, A. Neskakis, G. A. Varley, J. C. Willmott, F. Kearns, and J. C. Lisle, J. Phys. G **2**, 199 (1976).
[18] R. L. West, E. G. Funk, A. Visvanathan, J. P. Adams, and J. W. Mihelich, Nucl. Phys. A **270**, 300 (1976).
[19] C. A. Fields, K. H. Hicks, and R. J. Peterson, Nucl. Phys. A **440**, 301 (1985).
[20] C. Fahlander, I. Thorslund, B. Varnestig, A. Bäcklin, L. E. Svensson, D. Disdier, L. Kraus, I. Linck, N. Schulz, J. Pedersen, and D. Cline, Nucl. Phys. A **537**, 183 (1992).
[21] J. Ollier, Ph.D. thesis, University of Paisley (2004).
[22] B. Harmatz, T. H. Handley, and J. W. Mihelich, Phys. Rev. **128**, 1186 (1962).
[23] A. Tveter and B. Herskind, Nucl. Phys. A **134**, 599 (1969).
[24] M. Ohshima, E. Minehara, M. Ishii, T. Inamura, and A. Hashizume, Nucl. Phys. A **436**, 518 (1985).
[25] G. Gervais, D. C. Radford, Y. R. Shimizu, M. Cromaz, J. DeGraaf, T. E. Drake, S. Flibotte, A. Galindo-Uribarri, D. S. Haslip, V. P. Janzen, M. Matsuzaki, S. M. Mullins, J. M. Nieminen, C. E. Svensson, J. C. Waddington, D. Ward, and J. N. Wilson, Nucl. Phys. A **624**, 257 (1997).
[26] B. Singh and J. Chen, Nucl. Data Sheets **194**, 460 (2024).
[27] Coral M. Baglin, Nucl. Data Sheets **109**, 1103 (2008).
[28] B. Singh and J. Chen, Nucl. Data Sheets **191**, 1 (2023).
[29] R. Bengtsson and S. Frauendorf, Nucl. Phys. A **327**, 139 (1979).
[30] R. Bengtsson, J. Phys. **41**, C10 (1980).
[31] A. Bohr and B. R. Mottelson, *Nuclear Structure, Single Particle Motion* (Benjamin, New York, 1975), Vol. 1.
[32] G. Audi and A. H. Wapstra, Nucl. Phys. A **595**, 409 (1995).

[33] O. C. Kistner, A. W. Sunyar, and E. der Mateosian, Phys. Rev. C **17**, 1417 (1978).
[34] D. R. Bès, R. A. Broglia, and B. Nilsson, Phys. Lett. B **40**, 338 (1972).
[35] R. A. Broglia, D. R. Bès, and B. S. Nilsson, Phys. Lett. B **50**, 213 (1974).
[36] J. D. Garrett, G. B. Hagemann, B. Herskind, J. Bacelar, R. Chapman, J. C. Lisle, J. N. Mo, A. Simcock, J. C. Willmott, and H. G. Price, Phys. Lett. B **118**, 297 (1982).
[37] J. Simpson, M. A. Riley, J. R. Cresswell, D. V. Elenkov, P. D. Forsyth, G. B. Hagemann, D. Howe, B. M. Nyakó, S. Ogaza, J. C. Lisle, and J. F. Sharpey-Schafer, J. Phys. G: Nucl. Phys. **13**, 847 (1987).
[38] R. Bengtsson, S. Frauendorf, and F.-R. May, At. Data Nucl. Data Tables **35**, 15 (1986).
[39] K. Hara and Y. Sun, Int. J. Mod. Phys. E **04**, 637 (1995).
[40] K. Hara and Y. Sun, Nucl. Phys. A **529**, 445 (1991).
[41] K. Hara and Y. Sun, Nucl. Phys. A **537**, 77 (1992).
[42] Y. Sun, D. H. Feng, and S. X. Wen, Phys. Rev. C **50**, 2351 (1994).
[43] D. E. Archer, M. A. Riley, T. B. Brown, J. Döring, D. J. Hartley, G. D. Johns, T. D. Johnson, R. A. Kaye, J. Pfohl, S. L. Tabor, J. Simpson, and Y. Sun, Phys. Rev. C **52**, 1326 (1995).
[44] S.-X. Wen, H. Zheng, S.-G. Li, G.-S. Li, G.-J. Yuan, P.-F. Hua, P.-K. Weng, L.-K. Zhang, P.-S. Yu, C.-X. Yang, H.-B. Sun, Y.-B. Liu, Y.-Z. Liu, Y. Sun, and D. Hsuan Feng, Phys. Rev. C **54**, 1015 (1996).
[45] Y.-X. Liu, F.-Q. Chen, S.-Y. Yu, and Y. Sun, Sci. China: Phys., Mech. Astron. **58**, 1592 (2015).
[46] Y. Sun, Phys. Scr. **91**, 043005 (2016).
[47] J. A. Sheikh and K. Hara, Phys. Rev. Lett. **82**, 3968 (1999).
[48] Y. Sun, K. Hara, J. A. Sheikh, J. G. Hirsch, V. Velazquez, and M. Guidry, Phys. Rev. C **61**, 064323 (2000).
[49] Y. Sun, G.-L. Long, F. Al-Khudair, and J. A. Sheikh, Phys. Rev. C **77**, 044307 (2008).
[50] J. A. Sheikh, G. H. Bhat, Y. Sun, G. B. Vakil, and R. Palit, Phys. Rev. C **77**, 034313 (2008).
[51] Y.-X. Liu, C.-J. Lv, Y. Sun, and F. G. Kondev, J. Phys. G: Nucl. Part. Phys. **47**, 055108 (2020).